Tellus SERIES B CHEMICAL AND PHYSICAL METEOROLOGY
PUBLISHED BY THE INTERNATIONAL METEOROLOGICAL INSTITUTE IN STOCKHOLM

Tellus (2010)

TELLUS

Spatially simulating changes of soil water content and their effects on carbon sequestration in Canada's forests and wetlands

By WEIMIN JU[1,2]*, JING M. CHEN[2], T. ANDREW BLACK[3], ALAN G. BARR[4] and HARRY MCCAUGHEY[5], [1]*International Institute for Earth System Science, Nanjing University, 22 Hankou Road, Nanjing 210093, China;* [2]*Department of Geography, University of Toronto, Toronto, Ontario, Canada;* [3]*Department of Agricultural Science, University of British Columbia, Vancouver, BC, Canada;* [4]*Climate Research Branch, Meteorological Service of Canada, Saskatoon, SK, Canada;* [5]*Department of Geography, Queen's University, Kingston, Ontario, Canada*

(Manuscript received 17 September 2009; in final form 8 April 2010)

ABSTRACT

The variations of soil water content (SWC) and its influences on the carbon (C) cycle in Canada's forests and wetlands were studied through model simulations using the Integrated Terrestrial Ecosystem Carbon (InTEC) model. It shows that Canada's forests and wetlands experienced spatially and temporally heterogeneous changes in SWC from 1901 to 2000. SWC changes caused average NPP to decrease 40.8 Tg C yr^{-1} from 1901 to 2000, whereas the integrated effect of non-disturbance factors (climate change, CO_2 fertilization and N deposition) enhanced NPP by 9.9%. During 1981–2000, the reduction of NPP caused by changes in SWC was 58.1 Tg C yr^{-1} whereas non-disturbance factors together caused NPP to increase by 16.6%. SWC changes resulted in an average increase of 4.1 Tg C yr^{-1} in the net C uptake during 1901–2000, relatively small compared with the enhancement in C uptake of 50.2 Tg C yr^{-1} by the integrated effect of non-disturbance factors. During 1981–2000, changes in SWC caused a reduction of 3.8 Tg C yr^{-1} in net C sequestration whereas the integrated factors increased net C sequestration by 54.1 Tg C yr^{-1}. Increase in SWC enhanced C sequestration in all ecozones.

1. Introduction

Forests store more than 40% of the world's terrestrial carbon (C) (∼1150 Pg) (Prentice et al., 2001; Lal, 2005; Tarnocai et al., 2009) and have been considered to be a possible C sink, particularly in the Northern Hemisphere. Several factors have been hypothesized to contribute to this sink, including increased productivity by forests as a result of nitrogen (N) deposition (Holland et al., 1997), CO_2 fertilization (Schimel et al., 2000), interannual variability of climate (favouring either increased photosynthesis or decreased respiration) (Dai and Fung, 1993; Goulden et al., 1996; Dunn et al., 2007), longer growing season (Black et al., 2000), and land-use change (Brown and Schroeder, 1999; Caspersen et al., 2000). The understanding of the effects of these factors on terrestrial C cycling is crucial for projecting the future growth rate of atmospheric CO_2 concentration and for mitigating the impact of climate change through increasing terrestrial C storage.

C dynamics in terrestrial ecosystems are tightly linked with the water cycle. Two major components of the terrestrial C cycle (C assimilation through photosynthesis and C release through heterotrophic respiration) are both regulated by soil water content (SWC). Photosynthesis peaks when SWC is at field capacity and decreases with the departure of SWC from the optimum. Photosynthesis can totally diminish under very dry soil conditions. Extensive studies have demonstrated the dependence of C assimilation on SWC at leaf (Lawlor, 1995; Infante et al., 1999) and canopy (Reichstein et al., 2002; Rambal et al., 2003; Kljun et al., 2006; Ciais et al., 2005) levels. For example, the heat and drought in Europe in 2003 caused a 30% reduction in the continental gross primary productivity (GPP) (Ciais et al., 2005). However, the response of soil respiration to changes in SWC is not straightforward. SWC has no or little effect on heterotrophic respiration within a certain medium range, but is important at higher or lower SWC values. Modellers usually

*Corresponding author.
e-mail: juweimin@nju.edu.cn
DOI: 10.1111/j.1600-0889.2010.00459.x

assume that heterotrophic respiration peaks when SWC is at 0.6 of the total soil porosity (Friend et al., 1997; Frolking et al., 2001). The different reactions of heterotrophic respiration to changes in SWC in well-drained and poorly drained soils have been observed (Barr et al., 2004; Dunn et al., 2007). Within the same study area, Davidson et al. (1998) reported that soil respiration decreased in well-drained soils and increased in poorly drained soils during dry summers, whereas opposite results were found for wet summers. The range of optimum soil moisture values for heterotrophic respiration decreases with increasing temperature and the variation in SWC potentially becomes more important at higher temperatures (Borken et al., 2003).

Occupying approximately 417.6 and 127 million hectares of the land surface, Canada's forests and wetlands are an important component of the global terrestrial C cycle. Canada's forests contain about 13 Pg C in aboveground biomass (Kurz et al., 1992) and 38.6 Pg C in soils, excluding peaty organic soils (Siltanen et al., 1997). C stocks in wetlands are generally 5–50 times larger than those in upland ecosystems (Rapalee et al., 1998), with most stored in old and deep organic C layers (Trumbore and Harden, 1997). The estimated total of soil C in Canada's wetlands is about 168.4 Pg C. Studies indicated that Canada's forests acted as a C sink in the 20th century. The estimates of C sequestrated by Canada's forests during the 1980s and 1990s are not consistent, varying from a small C source of 12–14 g C m^{-2} yr^{-1} (Kurz and Apps, 1999) to a small C sink of 12–14 g C yr^{-1} (Chen et al., 2000a, 2003). Boreal and subarctic wetlands accounting for 20% and 30% of the northern landscape, respectively (Zoltai et al., 1988a,b) and have been hypothesized to be persistent C sinks, averaging 20–30 g C m^{-2} yr^{-1} over the past 5000 to 10 000 years (Tolonen et al., 1992; Gorham, 1995; Rapalee et al., 1998).

Long-term eddy covariance records show that C sequestration in Canada's forests and wetlands is very sensitive to soil drought (Lafleur et al., 2003; Humphreys et al., 2004; Kljun et al., 2006; Dunn et al., 2007). The response of C sequestration to SWC changes depends on ecological conditions. GPP of an aspen forest is more sensitive to drought than that of black spruce and jack pine forests in the Boreal Ecosystem-Atmosphere Study (BOREAS) Southern Study Area (SSA) near the Prince Albert National Park, Saskatchewan, Canada (Kljun et al., 2006). At the moderately well drained aspen forest site, the increase in SWC enhances heterotrophic respiration. The opposite relationship between heterotrophic respiration and soil wetness has been found at poorly drained sites. At a black spruce forest with a waterlogged soil in the Northern Study Area (NSA) of BOREAS, soil wetting caused this forest to shift from a small source to a small sink of C in recent years (Dunn et al., 2007). Drought might cause a decrease in daytime C uptake and an increase in nighttime soil C efflux at an ombrotrophic bog, east of Ottawa, Canada (Lafleur et al., 2003).

In the 20th century, Canada's forests and wetlands experienced spatially and temporally heterogeneous climate changes (Zhang et al., 2000). From 1900 to 1998, the annual mean temperature increased between 0.5 and 1.5 °C and annual precipitation increased from 5% to 35% in southern Canada (south of 60°N). From 1950 to 1998, the pattern of temperature change is distinct: warming in the south and west and cooling in the northeast. The increase in precipitation across Canada was in the range from 5% to 35% during this period, with significant negative trends found in southern regions during winters (Zhang et al., 2000). Annual mean streamflows decreased in most areas of Canada during 30–50 years prior to 1996 (Zhang et al., 2001), implying a change in the regional water balance during this period. However, the impact of climate-induced changes in surface water cycle on regional C balance has not yet been studied.

The main purposes of this study are (1) to examine whether Canada's forests and wetlands experienced ecologically significant changes in SWC in the last century, and (2) to assess the effects of these changes on C sequestration. To fulfill these purposes, simulations were conducted for the period during 1901–2000 using the Integrated Terrestrial C-Budget model (InTEC). The model was calibrated and validated using evapotranspiration (ET) measured using eddy covariance technique and unregulated streamflow measurements prior to the simulations conducted for the whole country.

2. Model description

The InTEC model was originally designed to simulate C balance for Canada's forests in the lumped mode (Chen et al., 2000b). Then, a series of modifications have been made for the model (Chen et al., 2003; Ju and Chen, 2005; Ju et al., 2007). The model currently consists of three components, a photosynthesis model for simulating historical annual net primary productivity (NPP), a soil model adopted from the CENTURY for simulating soil C and N dynamics (Parton et al., 1993), and a three-layer hydrological model for simulating monthly soil temperature, SWC, and water table depth (Ju and Chen, 2005). Through temporally and spatially upscaling the instantaneous leaf-level Farquhar biochemical model to the canopy level, the photosynthesis model quantifies the integrated effects of changes in stand age, climate, CO_2 and N deposition on the interannual variability of NPP to progressively calculate historical annual NPP from the initial NPP value (Chen et al., 2000b; Ju et al., 2007). The NPP value in a reference year (currently 1994), simulated at daily time steps using the Boreal Ecosystem Productivity Simulator (BEPS) model (Liu et al., 2002), is used as a benchmark to tune the initial NPP value. For each pixel, the initial NPP value is repeatedly adjusted until the difference between NPP simulated by InTEC and that output from BEPS in the reference year is less than 1%. A detailed introduction to photosynthesis model is given in Appendix A.

The hydrological model simulates SWC and temperatures of three soil layers at monthly time steps for quantifying the

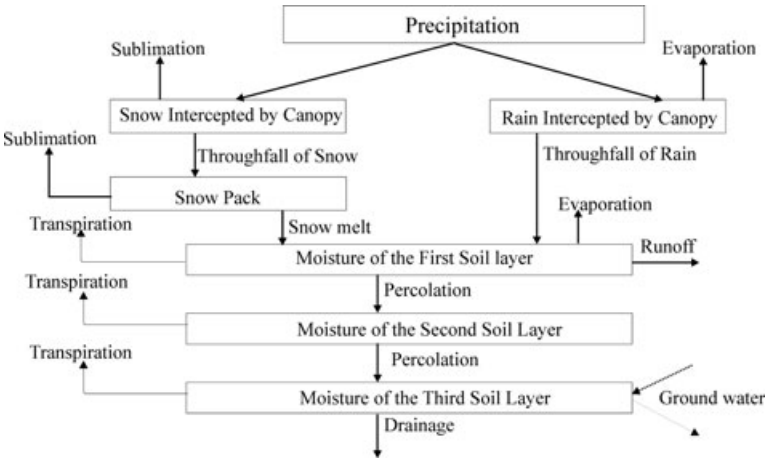

Fig. 1. Overview of the hydrological model used in this study. It simulates soil moisture content at monthly time steps. Vertical percolation is simulated with an implicit solution of Darcy's equation. Lateral saturated subsurface flow is simulated using the TOPMODEL scheme.

decomposition rates of soil C pools and soil water stress effect on photosynthesis (Fig. 1). The parameterization of this model is based on fractions of sand, clay, silt and organic matter (Saxton et al., 1986; Campbell and Norman, 1998; Letts et al., 2000) and vegetation properties. Water table is simulated according to the saturation degree of soils (Letts et al., 2000). Precipitation is partitioned into rainfall and snowfall according to air temperature (Davis et al., 1999). Transpiration is calculated as the total of water transpired from sunlit and shaded leaves using the Penman–Monteith formulation (Liu et al., 2003). Vertical water fluxes in the soil profile are calculated by implicitly solving Darcy's equation. The horizontal redistribution of soil water via saturated subsurface flow is determined according to the local topographic gradient following the TOPMODEL approach (Wigmosta et al., 1994). Formulations used in this hydrological model are given in Appendix B.

Temperatures of snowpack and soil are simulated using Fick's law of heat diffusion (Appendix C). To keep simulated temperatures stable at monthly time steps, the heat diffusion equation is implicitly solved. Thermal properties of snow and soil are estimated according to snow density, soil texture and SWC. The upper boundary condition of the heat diffusion equation is set according to air temperature with the consideration of canopy density (Yin and Arp, 1993). The bottom boundary condition is determined with the assumption that heat flux is zero at the bottom of soil profile. Simulated soil temperatures in conjunction with SWC are used to determine the decomposition rates by downscaling from the inherent maximum decomposition rates of various soil C pools (Ju and Chen, 2005).

Soil C and N dynamics are simulated using the modified approach of CENTURY (Parton et al., 1993). The model stratifies vegetation C into four pools (foliage, stem, fine root and coarse root) and soil C into nine pools (surface structural litter, soil structural litter, woody litter, surface metabolic litter, soil metabolic litter, surface microbial, soil microbial, slow and passive). The sizes of these C pools are updated at the end of each year.

The spin-up of the model is conducted using the average climatology from 1901 to 1910. Different procedures are followed to initialize C pools of forests and wetlands (Ju and Chen, 2005). For forests, the initialization is conducted by running the model until C pools reach an equilibrium state in 1900 (for stand age smaller than 100 in 2000) or in the year prior to the latest disturbance (for stand age larger than 100 in 2000). For wetlands, the initialization assumes the steady C dynamics for biomass and 'fast' soil C pools but not for 'slow soil C pools'. The slow and passive soil C pools are allowed to continuously increase and their initial values are set following Frolking et al. (2001) with an integrated period of 100 years for the slow C pool and 8000 years for the passive pool. After the initialization of soil C pools, the model is driven by the historical climate, CO_2 and N deposition from 1901 to 2000.

The InTEC model has been validated and used in several studies: (1) to estimate the historical trend of C balance in Canada's forests (Chen et al., 2000a); (2) to analyse the spatial patterns of current C sources and sinks in Canada's forests (Chen et al., 2003); (3) to simulate the spatial distribution of soil C stocks in Canada's forest and wetlands (Ju and Chen 2005); (4) to investigate the hydrological effects on C balance of Canada's forests and wetlands (Ju et al., 2006) and (5) to study the response of soil C in Canada's forests and wetlands to disturbance and climate change (Ju and Chen, 2008). In this study, validated using unregulated streamflow measurements at watershed scales, the InTEC model was employed to investigate the changes of SWC and corresponding effects on carbon sequestration by Canada's forests and wetlands during the period from 1901 to 2000.

3. Data used

Inputs to the InTEC model include spatial datasets of climate, soil texture, N deposition, leaf area index, land cover, forest stand age in 2000 and NPP simulated by the daily BEPS model in 1994, drainage and the Digital Elevation Model (DEM). Prior to or during the model execution, all spatial datasets were interpolated

into 1 km resolution with a standard Lambert conformal conic (LCC) projection (49°N and 77°N standard parallels and a 95°W meridian).

Remotely sensed data are used for deriving leaf area index, land cover and fire scar from which forest stand age in 2000 is inferred. In the land cover map (Cihlar et al., 1998), there are 31 cover types in total. Cover types from 1 to 15 are forests and wetlands and are grouped into four classes. Coefficients of NPP allocation to biomass pools and the turnover rates of biomass pools are specifically parameterized for each class (Chen et al., 2003). Forest stand age in 2000 was derived from the VEGETATION data, Canadian large-fire polygon and forest inventory databases (Amiro and Chen, 2003; Chen et al., 2003). With the assumption that forest started to regenerate in the next year following disturbance, the time of the latest disturbance was determined as 1999 minus the stand age in 2000. After forest regeneration, the stand age progressively increased until 2000. Prior to disturbance, forest was assumed to be at an equilibrium age. Under this situation, the productivity of forest did not vary without changes in climate, CO_2 concentration and N deposition. Forests were assumed to have a life cycle of 400 years and the model was repeatedly forced with the averages of climate, CO_2 and N deposition during 1901–1910 and normalized productivity changing with stand age. The equilibrium age was determined as the age, at which the C balance was in equilibrium.

Gridded monthly climate data, including mean air temperature, water vapour pressure and precipitation at 1 km resolution, were interpolated from the 0.5° global data produced by the U.K. Climate Research Unit from available station observations (New et al., 1999, 2000). Monthly mean radiation was estimated from the monthly mean temperature range, water vapour pressure and precipitation (Thornton and Running, 1999). Atmospheric deposition is an important N input to boreal forests. N deposition measurements for Canada's forests during 1983–1994 made by the Canadian Air and Precipitation Monitoring Network (CAPMN) (Ro et al., 1995) were spatially interpolated and extrapolated to produce a N deposition map in Canada. The historical annual N deposition values of each pixel were temporally extrapolated according to this N deposition map and historical national greenhouse gas emission (Chen et al., 2003). Drainage and soil texture (fractions of sand, silt, clay and organic matter) were compiled from the Soil Landscape of Canada (SLC) database (Schut et al., 1994). The 30 arcsec DEM data used here was derived from the cells of the Canadian Digital Elevation Data at the 1:250,000 scale by the Canadian Forest Service.

In this study, the model was further validated at stand and watershed scales. Monthly ET compiled from half-hourly eddy-covariance records at four forest sites were used for this purpose. Three of the sites are located in the BOREAS SSA, including a 73-year-old aspen site (SOA) (53.628°N, 106.198°W) (Black et al., 1996; Barr et al., 2004), a 121-year-old black spruce site (SOBS) (53.987°N, 105.118°W) (Jarvis et al., 1997; Arain et al., 2002) and a 65-year-old jack pine site (SOJP) (53.916°N, 104.692°W) (Griffis et al., 2003). The fourth site is a 53-year-old Douglas-fir forest (DF) (49.850°N, 125.317°W) on Vancouver Island, BC (Humphreys et al., 2003). To investigate the ability of the model to simulate SWC at regional scale, simulated watershed-scale runoff was compared with measured annual mean streamflow records in the HYDAT CD-ROM database from Environment Canada. This database contains hydrometric data for over 2900 active stations and some 5100 discontinued sites across Canada. Only stations with more than 20years of unregulated streamflow records were selected. There are 84 unregulated stations in total used for the purpose of model validation.

4. Model simulations and detection of trends of soil water content

4.1. Model simulations

Five simulations were conducted for the period from 1901 to 2000 (Table 1). In Simulation I, the model was forced by the baselines of climate, CO_2 and N deposition and changing stand age during the entire simulation period. These baselines are their average values over the 1901–1910 period. In this simulation, we attribute the changes in C balance to the effect of stand age change. In Simulation II, historical atmospheric CO_2 concentration, changing stand age and the baselines of climate and N deposition were used to force the model. This simulation is made to investigate the effect of CO_2 fertilization on C balance. In Simulation III, N deposition and stand age changed with time whereas climate and CO_2 concentration remained at their respective baselines. This simulation allows quantification of the effect of increasing N deposition on C balance. In Simulation

Table 1. Description of five simulation experiments

Simulation	Temperature	Precipitation	Radiation	Water vapor pressure	SWC	CO_2	N deposition
I	Baseline	Baseline	Baseline	Baseline	Baseline	Baseline	Baseline
II	Baseline	Baseline	Baseline	Baseline	Baseline	Historical	Baseline
III	Baseline	Baseline	Baseline	Baseline	Baseline	Baseline	Historical
IV	Historical	Historical	Historical	Historical	Historical	Historical	Historical
V	Historical	Baseline	Baseline	Historical	Baseline	Historical	Historical

Table 2. Parameter values used for different land cover types

Cover type	Deciduous	Conifer	Mixed	Shrub	Crop	Grass	Other
Clumping index (unitless)[a]	0.8	0.5	0.65	0.8	0.9	0.9	0.9
Aerodynamic resistance (s m^{-1})[a]	5	5	5	5	30	30	30
Vmax at 25 °C (μmol m^{-2} s^{-1})[b,c,d,e]	60	33	40	60	90	60	30
Maximum stomatal conductance (m s^{-1})[b,f]	0.006	0.0016	0.0025	0.006	0.008	0.006	0.002

[a]Liu et al. (2003).
[b]Chen et al. (1999).
[c]Arain et al. (2002).
[d]Kucharik et al. (2000).
[e]Arora (2003).

IV, climate (temperature, precipitation, radiation, water vapour pressure), CO_2, N deposition and stand age changed with time. In this way, the combined effects of disturbance and nondisturbance factors on C balance of Canada's forests and wetlands are simulated. In Simulation V, SWC and precipitation were kept at the averages during 1901–1910 whereas other environmental factors and stand age changed with time. The difference in C balance between Simulations IV and V is therefore caused by the variations of SWC.

In all simulations, C pools, SWC, soil temperature and NPP are initialized using the same methods. The values of some model parameters and their sources used in this study are listed in Table 2.

4.2. Detection of temporal trends of soil water content

The temporal changes of SWC in the 20th century were detected using the Mann–Kendall test (Mann, 1945; Kendall 1975) for all pixels in Canada's forests and wetlands. This test is a non-parametric test widely used to assess trends in climatology and hydrology (Zhang et al., 2000, 2001).

5. Results

5.1. Validation of simulated evapotranspiration and streamflow

To validate the model simulations of water vapour fluxes from land surface to the atmosphere, simulated monthly ET was compared with eddy covariance measurements at four forest sites (Fig. 2). The model is able to reproduce seasonal patterns of ET well. In SSA, the agreements between simulated and measured monthly ET are 92.8% for the SOA forest during January 1999 to December 2000, 88.5% for the SOJP forest during August 1999 to December 2000, and 90.2% for the SOBS forest during April 1999 to December 2000, respectively. The root

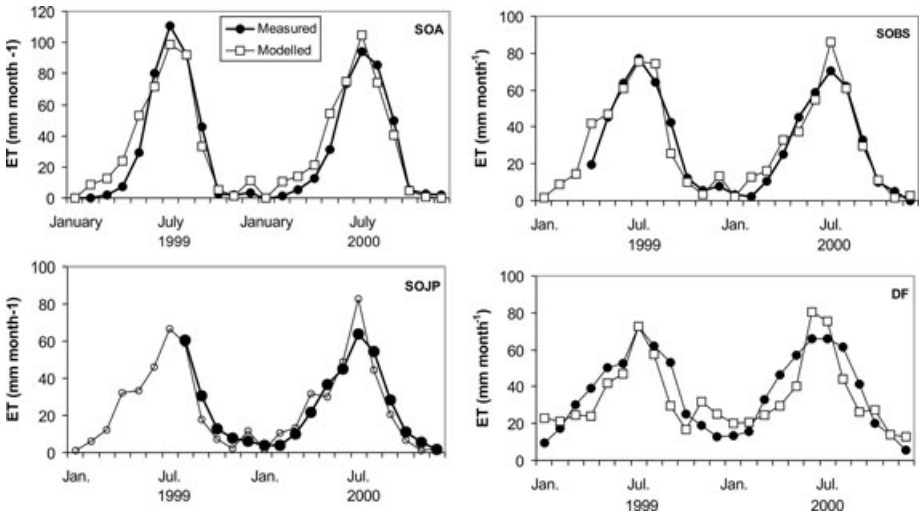

Fig. 2. Comparison of monthly evapotranspiration (ET) between simulated results and eddy covariance measurements for three forests at the southern study area of the Boreal Ecosystem Atmosphere Study (BOREAS), Saskatchewan, Canada, and a forest on the Vancouver Island, British Columbia, Canada. SOA, Southern Old Aspen forest; SOBS, Southern Old Black Spruce forest; SOJP, Southern Old Jack Pine forest; DF, Douglas-Fir forest.

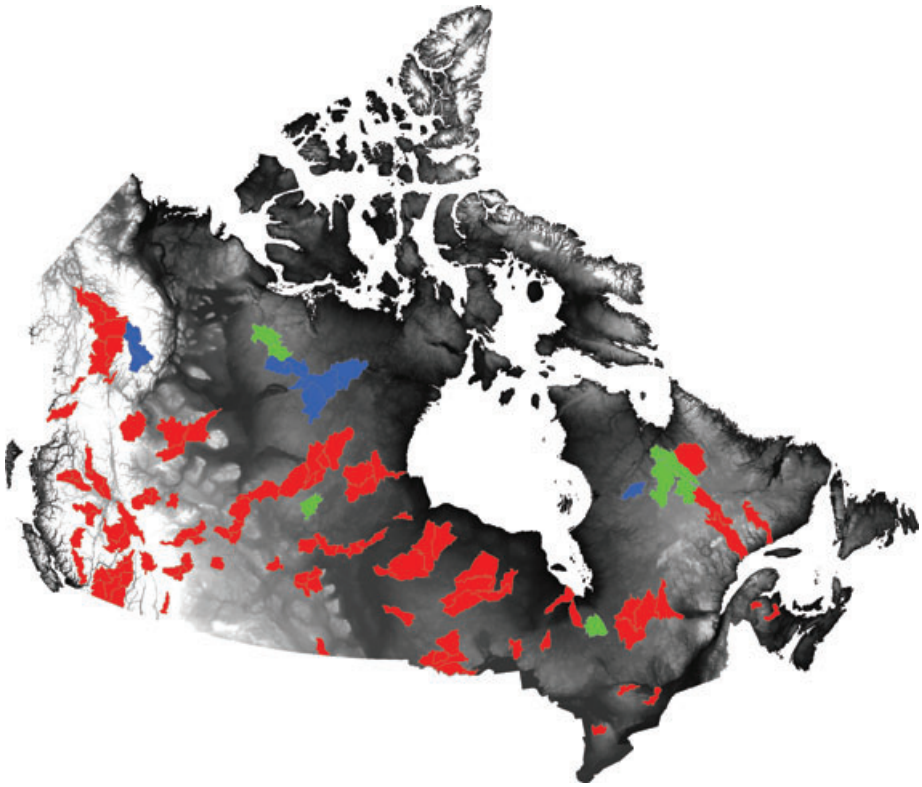

Fig. 3. Locations of drainage basins used for validation of simulated streamflows. The red and green colours indicate that there is correlation between measured and simulated annual mean streamflow values at the 1% and 5% significance levels, respectively, whereas the blue colour indicates no significant correlation between measured and simulated annual mean streamflow values.

mean square errors (RMSE) of monthly simulated ET are 10.6, 8.1 and 8.7 mm m^{-1} at these three sites. However, the model tends to underestimate ET in spring and autumn and overestimate ET in winter for the Douglas-fir forest on the Vancouver Island. The model only explained 71.3% of monthly ET variations during January 1999 to December 2000, with an RMSE of 11.7 mm m^{-1}.

The simulated runoff (including surface runoff and vertical drainage from the bottom of soil profile) at the watershed level was compared with streamflow measurements at hydrometric stations, which have unregulated streamflow records more than 20 years. A total of 84 stations were selected across the country (Fig. 3). The contributing areas to these stations range from 1230 to 65 600 km^2. Some stations receive water from several watersheds. In these cases, runoff from contributing areas to the river channels was summed in order to be compared with streamflow measurements. Simulated annual mean stream flows for these stations are in good agreement with measured values, with 74 stations having R^2 at the 0.01 significance level (red coloured areas in Fig. 3) and four stations at the 0.05 significance level (green-coloured areas in Fig. 3). The maximum R^2 is 0.79 ($N = 29$) (Table 3). Table 3 also shows the slopes and intercepts of regression between simulated and observed streamflow with observation as X and simulations as Y. At all stations, slopes are smaller than unity, indicating that the model tended to underestimate high streamflow values. It means that SWC might be overestimated in years with high streamflow. Consequently, C sequestration might be overestimated in poorly drained areas and underestimated in well-drained areas.

The agreement between simulated and measured streamflows generally decreases from south to north. The six stations, at which the correlation between simulated and measured annual mean streamflow values is not significant (blue coloured areas in Fig. 3), are located in the northern areas. Simulated interannual variability of stream flow is mostly smaller than that in the observational records. The standard deviation values of simulated annual mean streamflows are in the range of 50–80% of those calculated from streamflow measurements.

5.2. *Trends in simulated evapotranspiration and soil water content*

Simulated annual ET exhibits an increasing gradient from north to south and is significantly different in various ecozones (Fig. 4 and Table 4). The north-south gradient of ET is similar to the spatial patterns of air temperature and incoming solar energy available for driving water flux from ground surface to the atmosphere. Average annual ET is less than 200 mm yr^{-1} in the

Table 3. Statistics from the regression ($Y = aX + b$) of simulated (as Y) on observed (as X) annual mean streamflow ($m^3\ s^{-1}$)

No	Pro.	Lat. (°N)	Lon. (°W)	Area (km^2)	R^2	RMSE ($m^3 s^{-1}$)	Years	a	b	No	Pro.	Lat. (°N)	Lon. (°W)	Area (km^2)	R^2	RMSE ($m^3 s^{-1}$)	Years	a	b
1	NB	47.832	66.882	2270	0.45	7.1	71	0.80	14.8	43	MB	53.786	97.672	4610	0.51	7.5	19	0.42	16.6
2	NB	46.736	65.827	5050	0.62	14.0	53	0.56	21.9	44	MB	56.519	94.206	3290	0.49	6.2	26	0.55	12.2
3	ON	48.012	89.616	1550	0.52	5.9	76	0.76	8.6	45	AB	54.354	110.217	14500	0.48	12.9	45	0.29	19.8
4	ON	48.774	86.297	4270	0.30	16.9	30	0.74	63.5	46	SK	57.089	103.711	10200	0.31	29.8	23	0.37	62.5
5	ON	44.456	81.327	3960	0.56	16.7	86	0.58	16.7	47	MB	58.892	96.275	48100	0.26	96.3	37	0.26	198.0
6	ON	43.132	80.267	5210	0.75	10.4	62	0.52	20.5	48	NU	64.530	101.362	65600	0.10	129.6	28	0.12	178.3
7	ON	44.254	77.419	2620	0.44	11.9	85	0.65	20.8	49	NU	61.254	100.974	21400	0.35	41.9	30	0.35	77.6
8	ON	45.888	77.308	4120	0.47	24.3	85	0.74	34.6	50	AB	54.451	113.992	13100	0.60	34.0	39	0.41	30.2
9	ON	45.328	77.514	5800	0.60	33.4	70	0.91	34.1	51	AB	56.685	111.254	30800	0.51	34.1	42	0.51	67.6
10	ON	45.177	76.124	2900	0.41	14.3	82	0.61	23.6	52	AB	55.072	118.803	11300	0.52	22.2	40	0.46	62.7
11	QC	46.584	72.405	4480	0.61	15.9	29	0.71	39.7	53	AB	55.457	117.161	11100	0.64	17.2	40	0.35	23.2
12	QC	48.686	72.488	15300	0.40	34.7	34	0.59	103.6	54	SK	59.147	105.539	50700	0.25	18.2	34	0.45	185.4
13	QC	50.350	66.190	19000	0.48	51.3	28	0.44	214.9	55	NT	60.743	115.858	47900	0.52	44.5	37	0.40	87.0
14	QC	50.308	63.623	13000	0.38	44.2	38	0.49	166.8	56	NT	62.895	108.468	26600	0.10	31.3	34	0.32	84.4
15	QC	49.858	77.187	31900	0.48	76.1	28	0.62	167.4	57	BC	58.072	130.824	3600	0.62	9.3	33	0.67	8.8
16	QC	49.753	77.614	22200	0.63	71.6	33	0.55	117.7	58	BC	56.739	131.674	9350	0.46	67.8	34	0.74	68.3
17	QC	55.684	74.340	10400	0.10	48.9	32	0.25	29.8	59	BC	54.618	126.899	7360	0.52	30.6	53	0.71	65.5
18	QC	57.429	69.208	48500	0.21	436.8	33	0.18	1258.3	60	BC	54.085	124.599	6030	0.40	11.5	47	0.30	29.2
19	QC	57.883	67.583	29800	0.34	125.8	33	0.45	232.9	61	BC	54.416	124.269	14600	0.52	38.1	58	0.50	32.2
20	NF	54.455	66.625	19000	0.37	116.1	45	0.36	156.3	62	BC	54.079	121.848	18000	0.49	73.3	47	0.61	121.6
21	MB	55.850	92.099	65500	0.37	161.1	22	0.34	214.5	63	BC	54.096	122.678	4300	0.54	6.1	40	0.73	10.7
22	ON	54.517	87.233	50000	0.55	308.4	27	0.45	484.1	64	BC	53.311	122.888	12400	0.47	12.2	30	0.31	14.8
23	ON	53.092	85.008	36000	0.79	152.6	29	0.64	180.0	65	BC	52.844	122.224	11500	0.51	49.2	53	0.81	19.3
24	ON	51.150	80.867	4250	0.32	41.3	29	0.81	46.6	66	BC	51.656	120.065	10200	0.44	30.3	59	0.74	39.7
25	ON	49.617	83.263	8940	0.43	32.7	80	0.42	32.5	67	BC	50.938	119.654	3080	0.48	9.1	69	0.79	12.8
26	ON	51.083	80.767	6680	0.39	19.2	34	0.60	45.3	68	BC	50.765	119.740	16200	0.52	42.7	71	0.78	66.1
27	QC	49.985	79.095	11200	0.31	49.8	18	0.48	112.7	69	BC	50.330	121.226	7280	0.44	11.6	39	0.76	14.9
28	AB	52.028	114.139	2560	0.23	3.5	40	0.36	5.7	70	BC	52.070	123.537	6940	0.28	23.2	48	0.53	22.7
29	AB	52.277	113.816	11600	0.41	18.1	83	0.31	33.6	71	BC	49.311	121.802	7870	0.56	47.1	47	0.71	102.6
30	AB	53.787	113.223	3350	0.54	22.7	75	0.24	26.2	72	BC	51.483	117.179	9710	0.60	26.1	54	0.72	26.9
31	AB	52.708	111.310	3500	0.35	3.8	37	0.20	4.7	73	BC	49.510	115.071	3110	0.74	6.7	31	0.70	11.2
32	SK	53.213	105.885	5100	0.32	17.6	31	0.23	22.1	74	BC	49.378	120.152	5590	0.67	9.9	35	0.58	18.3
33	SK	53.136	104.021	4400	0.26	5.1	43	0.11	4.2	75	BC	48.931	119.419	8280	0.61	6.8	58	0.54	12.6
34	SK	53.417	103.142	9250	0.46	7.1	19	0.23	10.0	76	BC	48.984	118.215	9840	0.59	14.7	71	0.69	30.9
35	SK	54.439	102.175	14600	0.39	16.9	35	0.23	33.5	77	YT	62.830	136.581	49000	0.31	90.5	41	0.52	134.3
36	SK	52.860	102.194	11000	0.55	10.1	27	0.45	15.7	78	YT	60.050	128.900	33400	0.63	43.9	40	0.88	45.2
37	MB	49.060	101.050	3210	0.31	14.7	58	0.08	5.2	79	YT	60.474	129.119	12800	0.35	21.7	35	0.57	72.0
38	ON	48.383	92.178	13400	0.52	28.3	78	0.41	41.3	80	BC	58.788	122.659	20300	0.53	36.1	41	0.50	25.6
39	ON	48.850	92.725	4870	0.66	12.8	77	0.61	24.4	81	NT	61.530	125.411	8560	0.10	17.5	27	0.31	62.7
40	ON	49.875	91.458	6230	0.65	16.6	79	0.67	30.7	82	NT	61.636	125.795	14600	0.10	38.5	29	0.23	174.7
41	MB	51.703	96.604	9090	0.37	32.2	24	0.40	50.8	83	NT	66.790	133.082	18600	0.10	52.9	23	0.15	193.1
42	MB	55.743	97.000	15400	0.30	35.9	38	0.18	24.7	84	NT	65.414	114.008	19300	0.25	30.2	30	0.29	68.3

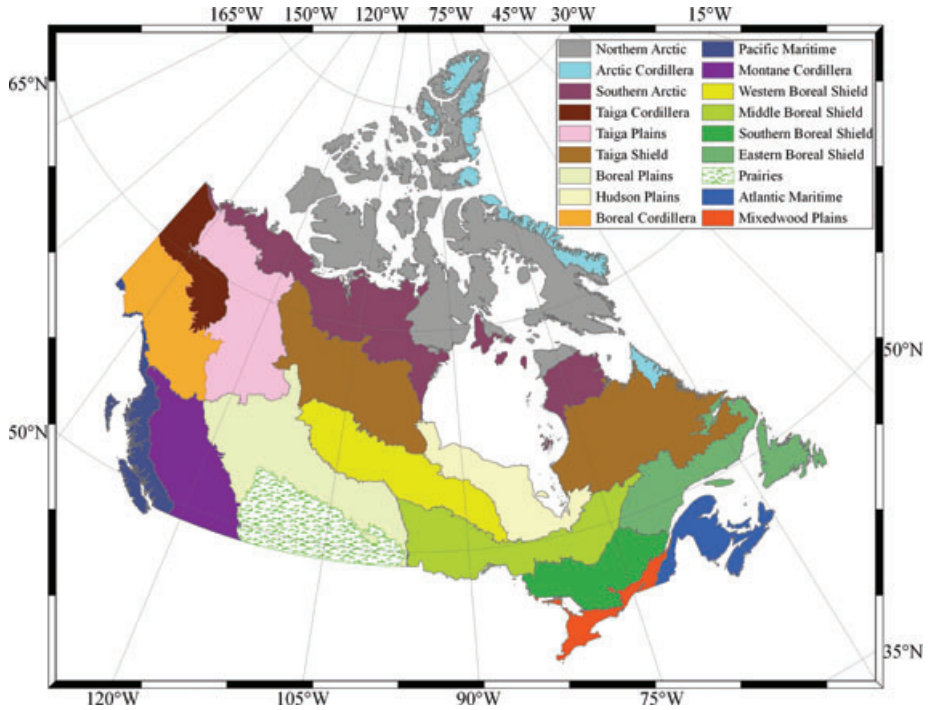

Fig. 4. Spatial distribution of various ecozones in Canada.

Table 4. Average annual evapotranspiration per ecozone during different periods in different ecozones

Ecozone	Annual ET (mm yr^{-1})		
	1901–1910	1945–1954	1991–2000
Boreal Plains	317	316	326
Boreal Cordillera	197	200	199
Western Boreal Shield	292	278	299
Middle Boreal Shield	351	342	357
Southern Boreal Shield	416	401	418
Eastern Boreal Shield	286	306	326
Atlantic Maritime	400	432	448
Mixewood Plains	420	423	426
Southern Arctic	102	110	120
Taiga Cordillera	119	130	129
Taiga Plains	229	242	253
Taiga Shield	191	191	213
Hudson Plains	265	259	286
Pacific Maritime	348	340	339
Montane Cordillera	320	352	334
Prairies	328	318	320

Southern Arctic and Taiga Cordillera ecozones whereas mean annual ET increases to about 400 mm yr^{-1} in the Southern Boreal shield, Mixedwood and Atlantic Maritime ecozones. In other ecozones, average annual ET ranges from 200 to 400 mm yr^{-1}. In the last century, annual ET increased in most ecozones of Canada, with a largest increase of 4×10^{-1} mm yr^{-1} in Eastern Boreal Shield.

SWC is a key factor determining the seasonal and interannual variability of C balance. Growing-season mean SWC simulated in Simulation IV changes at annual to decadal time scales. The patterns of decadal change in average SWC per ecozone are especially clear in the Taiga Shield, Taiga Cordillera, Taiga Plains and Boreal Plains ecozones. The temporal patterns of SWC changes are spatially heterogeneous (Fig. 5). In the Southern Arctic and Taiga Cordillera ecozones, SWC increased noticeably during the first 5 years. Then, SWC fluctuated without notable trends until the 1960s in the Southern Arctic ecozone. It gradually declined until the end of 1940s and then started to increase until the middle 1960s in the Taiga Cordillera ecozone. SWC did not show clear trends prior to the middle 1980s in the Hudson Plains, Eastern Boreal Shield and Mixedwood Plains ecozones. In other ecozones, SWC mostly declined in the 1910s and was lower in the 1920s. Soils became wetter during the late 1920s and early 1930s and drier again in years around 1940. SWC increased gradually from the middle 1940s to the early 1960s and declined from the early 1970s. Soils became drier in the 1990s in most regions except the Boreal Cordillera, Pacific Maritime and Montane Cordillera ecozones. SWC dropped dramatically in 1998, a year with the highest annual mean temperature. The long-term trends in SWC were affected by the temporal trends of climate data used to drive the model. During the period from 1901 to 2001, variations of temperature and precipitation in Canada were spatially heterogeneous. Temperature

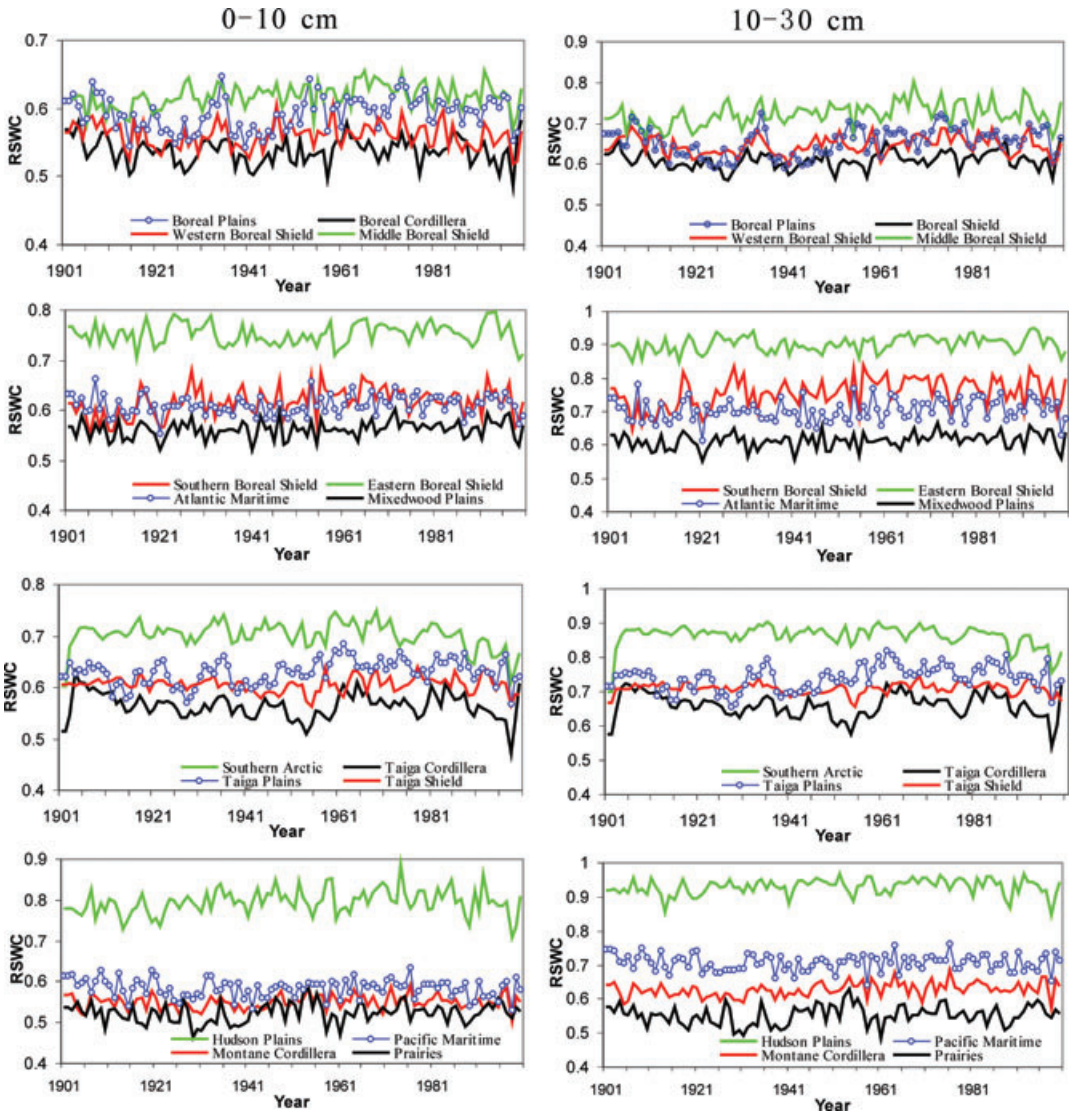

Fig. 5. Temporal changes of the ecozone mean growing-season (May to September) soil water content (fraction of porosity) at 0–10 cm (upper panel) and 10–30 cm (lower panel) depths in different ecozones of Canada.

increased in the south and west and decreased in the northeast. In areas south of Hudson Bay, temperature decreased by about 0.5 °C. Precipitation increased in most areas of Canada, ranging from 5% to 25%. The largest increases in precipitation occurred in areas of the Montane Cordillera and southeast to the Hudson Bay. In areas with increasing precipitation and less warming, SWC increased, and vice versa. If temperature will increase and precipitation will correspondingly decrease in the future, SWC will possibly decrease.

The Mann–Kendall test shows that SWC increased overall from 1901 to 2000 in most areas, especially in the Southern Taiga Plains, the Northwestern Boreal Plains, the Eastern Hudson Plains, the Eastern Middle Boreal shield ecozones and parts of the Southern Boreal Shield ecozone. In these areas, increasing trends of SWC were detected at the 1% significance level (red and pink areas in Fig. 6). The increase of SWC in these areas is due mainly to the excess of precipitation increases over ET increases. In other areas, SWC increased less or even decreased at the 1% significance level, for example, in parts of the Taiga Shield, Taiga Cordillera, Taiga Plains and Boreal Cordillera ecozones.

The test shows that SWC decreased extensively during 1971 to 2000 except in the Southern Taiga Plains, Western Taiga Shield, northwest Western Boreal Shield and Southern Boreal Shield ecozones (yellow colour in Fig. 6). In these areas, SWC increased in the last three decades of the 20th century, but not significant. The decreasing trends in SWC were significant at the 1% level in the Northern Taiga Plains and Southern Boreal Plains ecozones, and parts of the Hudson Plains, Southern Boreal Shield and Eastern Taiga Shield ecozones (green and blue areas

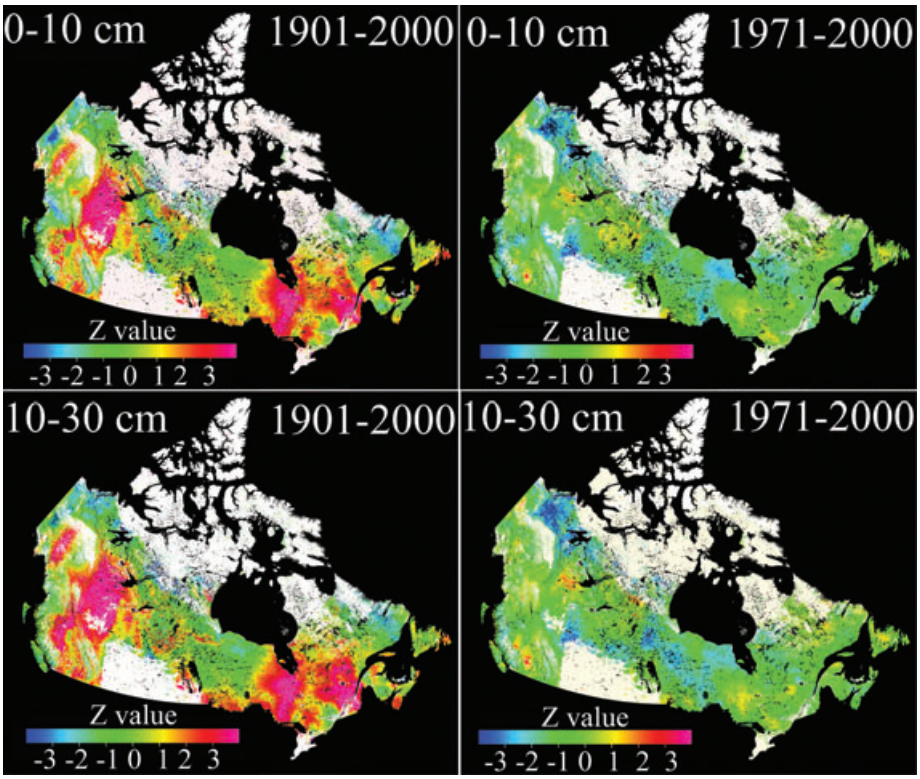

Fig. 6. Trends in simulated growing season mean volumetric soil water content at 0–10 cm (upper panel) and 10–30 cm (lower panel) depths during periods from 1901 to 2000 and from 1971 to 2000. A positive Z value means an increasing trend, and vice versa. If $|Z| > 1.96$, the trend is at the 5% significance level.

in Fig. 6). The drying trends in deeper and surface layers were similar in most areas, but slightly different in the Western Boreal Shield ecozone.

5.3. *Effects of changing soil water content on carbon balance*

In Simulation IV, stand age, CO_2, N deposition, climate change with time. In Simulation V, SWC and precipitation were kept at the baselines while stand age, CO_2, N deposition and other climate factors vary temporally. The difference of simulated C balance between Simulations IV and V is attributable to the effects of SWC change. Variations of SWC resulted in changes in NPP in Canada's forests and wetlands during 1901–2000 (Fig. 7). The average reduction in NPP was 40.8 Tg C yr^{-1} (8.1 g C m^{-2} yr^{-1}) (equal to NPP simulated in Simulation IV minus that simulated in Simulation V) over the period from 1901 to 2000. The reductions of NPP caused by SWC variations were most obvious in the Southern Taiga Plains, the Northwestern Boreal Plains, the Eastern Hudson Plains, the Eastern Middle Boreal shield ecozones and parts of the Southern Boreal Shield ecozone, ranging from 10 to 15 g C m^{-2} yr^{-1}. The SWC-induced reduction in national total NPP was exceeded by the integrated enhancement effects of warming, CO_2 fertilization and N deposition (Fig. 7). All environmental factors together caused an increase in NPP by 9.9% (83.4 Tg C yr^{-1} or 16.1 g C m^{-2} yr^{-1}) during 1901–2000 relative to NPP simulated with the baselines of climate, CO_2 and N deposition and with stand age variation. The enhancement effects of CO_2 fertilization and N deposition on NPP are 16.7 and 29.6 Tg C yr^{-1}, respectively, when averaged from 1901 to 2000. In the drying and wetting periods, NPP of well-drained upland forests and poorly drained forests and wetlands exhibited different responses to changes in SWC. During drying periods, NPP decreased in well-drained forests and increased in poorly drained forests and wetlands, and vice versa. The changes in growing-season temperature and length caused much larger interannual variability in NPP than SWC change did. The reduction in N mineralization due to soil wetting during the middle 1940s and the early 1970s resulted in a considerable decrease in NPP because of the sensitivity of photosynthesis to N availability in Canada's forests and wetlands. The decline in SWC after the middle 1970s stimulated N mineralization because of improved soil aerobic conditions. However, the reduction in stomatal conductance due to low SWC caused decrease in NPP in well-drained areas. During the period from 1981 to 2000, the reduction of NPP related to SWC variations was 58.1 Tg C yr^{-1} (11.6 g C m^{-2} yr^{-1}).

Soil water also affects C released from heterotrophic respiration resulting from soil C decomposition. The SWC-induced reduction in NPP was exceeded by the decrease in heterotrophic

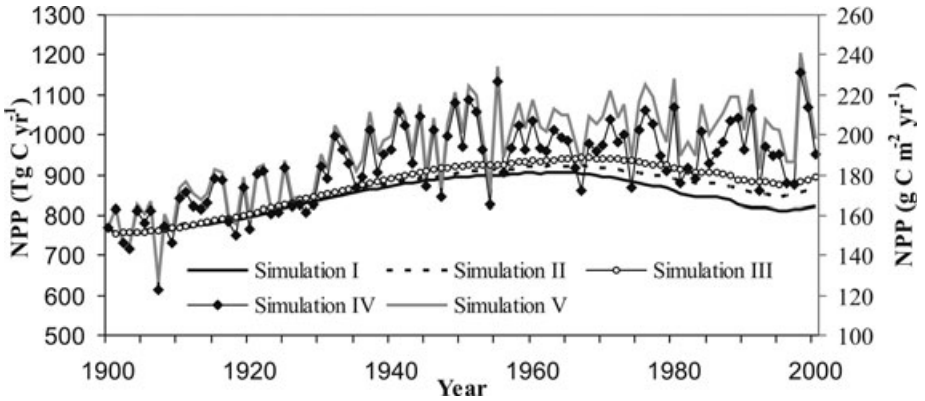

Fig. 7. Annual NPP values of Canada's forests and wetlands from five simulations. In Simulation I, only forest stand age changed with time and the baselines of climate, CO_2 and N deposition were used to run the model; In Simulation II, CO_2 concentration and stand age changed with time while climate and N deposition remained at the baseline values; In Simulation III, only N deposition and stand age changed with time while climate and CO_2 concentration remained at baseline values; In Simulation IV, historical climate, CO_2 and N deposition were used to drive the model and stand age changed with time also. In Simulation V, SWC was remained at the baseline while stand age, other climatic variables, CO_2 and N deposition change with time.

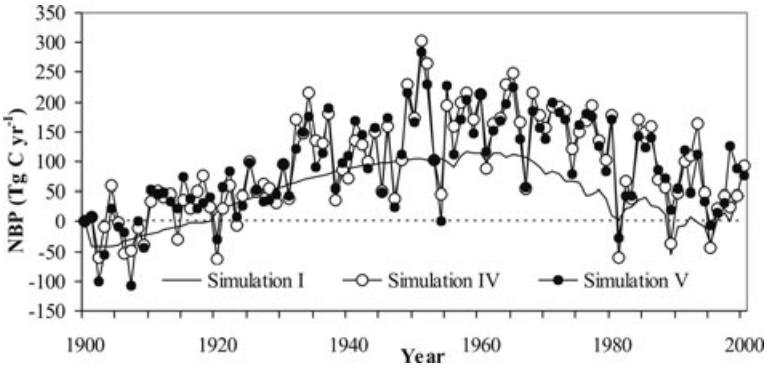

Fig. 8. Annual net biome productivity (NBP) in Canada's forests and wetlands output from three different Simulations (see Table 1 for the definition of Simulations).

respiration caused by SWC changes. Changes in SWC increased net biome productivity (NBP) of Canada's forests and wetlands by 4.1 Tg C yr^{-1} averaged over the simulation period. This number is relatively small compared with an increase of 50.2 Tg C yr^{-1} in NBP caused by the integrated effect of climate change, CO_2 fertilization and N deposition (Fig. 8). The effects of CO_2 and N deposition increased NBP by 13.3 and 16.3 Tg C yr^{-1}, respectively. Drought might simultaneously reduce C assimilation and heterotrophic respiration in well-drained upland forests and enhance C assimilation and heterotrophic respiration in poorly drained forests and wetlands. In contrast to drought, wetting of soils might affect C uptake in the opposite direction (Goulden et al., 1996; Dunn et al., 2007). The average reductions in C sequestration caused by SWC decrease were 3.9 Tg C yr^{-1} during 1906–1929 and 3.7 Tg C yr^{-1} during 1981–2000, respectively. The average increase in C sequestration related to SWC increase was 14.4 Tg C yr^{-1} during 1947–1970. During the period from 1981 to 2000, the reduction of C sequestration related to SWC variations was 3.8 Tg C yr^{-1} (0.7 g C m^{-2} yr^{-1}). The SWC-induced enhancement of NBP is due to the compensation between heterotrophic respiration and NPP.

Increases in SWC resulted in increases in NBP in all ecozones (Fig. 9). The change of SWC induced considerable interannual variability of NBP. The drought from the middle 1900s to the late 1930s caused the decrease in NBP mainly in Boreal Cordillera, Montane Cordillera, Southern Boreal Shield and Boreal Plains. Drying of soils in the 1980s and 1990s resulted in a widespread reduction in C sinks of Canada's forests and wetlands, especially in Southern Arctic, Taiga Shield, Taiga Cordillera, Taiga Plains, Middle Boreal Shield, Eastern Boreal Shield, Boreal plains, Hudson Plains and Mixedwood plains. In other ecozones, changes in SWC caused relatively small decreases in NBP. The model simulated a big decrease in NBP for all ecozones in 1998 with a very warm climate.

6. Discussion

Validations show that the model is able to capture the seasonal and interannual variations of ET. However, discrepancy between

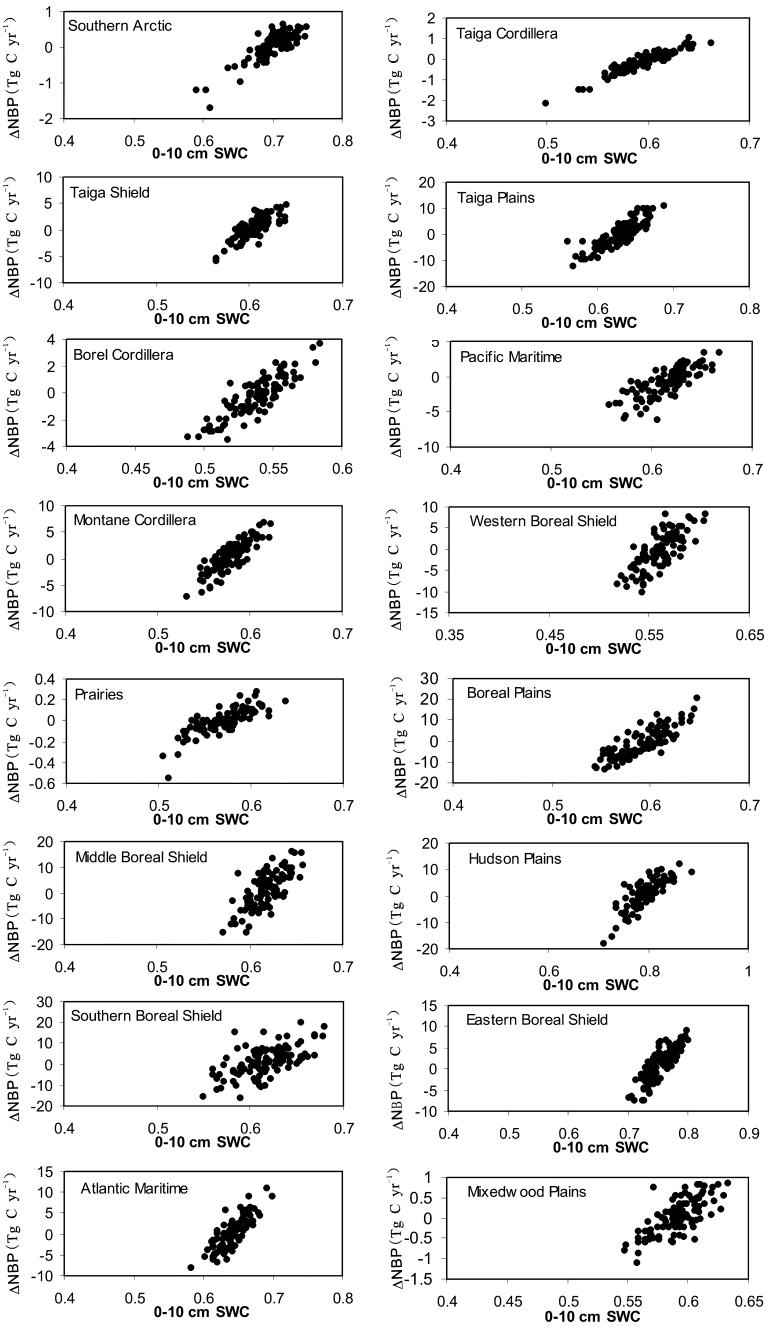

Fig. 9. Effect of changes in soil water content on NBP in various ecozones. ΔNBP is the difference in NBP between Simulations IV and V and represents the effect of changes in soil water content on NBP. Positive ΔNBP values mean that changes in soil water content cause the increase in NBP.

simulated and measured ET still exits. The errors in simulated ET may be related to uncertainties in the simulation of stomatal conductance, parameterization of hydrological model and estimation of canopy interception of rain. First, the species-dependent sensitivity of stomatal conductance to water vapour deficit has not been considered in this model. Secondly, the hydrological model is parameterized according to soil properties compiled from the SLC database. The vertical heterogeneity of hydrological parameters is not represented in the model. This simplification can introduce some errors in simulated SWC and ET. Thirdly, the model is run at monthly time steps and may have errors in the estimation of canopy interception of rainfall of various intensities. For the SOA and SOB sites, simulated ET is closer to the measured values in the second half of the growing-season than in the first half. The slight overestimation of ET by the model in the early growing season is possibly related to the

retarded root water uptake under low soil temperature. At these sites, soil temperature increases more slowly than air temperature in early spring due to the thermal insulation effect by thick organic C and litter layers. Low soil temperature retards root activity and consequently canopy transpiration. Inclusion of the effect of low soil temperature on root activities would improve the reliability of simulated ET.

Simulated annual ET exhibits an increasing gradient from north to south, mirroring the spatial patterns of temperature and solar energy available for vegetation growth and transpiration. In the last century, annual ET increased in most ecozones of Canada. The increasing trend exhibited distinguished spatial pattern, with a largest increase of 4×10^{-1} mm yr^{-1} in Eastern Boreal Shield. This implies a possible future increase of ET corresponding to global warming. If the increase in ET exceeds the increase in precipitation, SWC will decrease and C sequestration will be affected in Canada's forests and wetlands.

Uncertainty in simulated SWC is one of major sources resulting in errors in the estimation of regional C balance. However, it is very difficult to validate SWC at regional scale due to large spatial variability of SWC. In this study, long-term unregulated streamflow data across Canada were employed to evaluate uncertainties in simulated regional SWC. This is the first attempt in the study of regional C balance. The agreement between simulated and observed streamflows decreases from south to north. The discrepancy between simulated and measured streamflow might be attributed to following factors, including relatively coarse time steps, limited number of soil layers, improper representation of snowmelt and frozen/thawing processes of soils and uncertainties in precipitation data in the remote northern areas. In this study, this model operated at monthly time steps and had difficulties to capture peak streamflow produced by extreme rainfall events. Currently, the model stratified the soil profile into three layers. The errors in the determination of upper and lower boundary conditions of water fluxes will be propagated into simulated SWC and streamflow. With the increase of soil layers, errors in simulated SWC can be well constrained. However, the computation will be greatly increased. The simulated spring streamflow is sensitive to the timing of snowmelt. The model simulates snowmelt according to monthly mean air temperature and can only partially capture the interannual variability in the timing of spring snowmelt. The effects of frozen/thawing processes on soil water movement were currently considered by reducing hydraulic conductivity with temperature using an empirical function, which needs further refinement. In addition, measurements of precipitation in the remote northern areas are limited. Uncertainties in precipitation data used to force the model would be definitely propagated into simulated streamflow and SWC, resulting in larger discrepancy between simulated and measured streamflow in the north than in the south. Further efforts are required to improve the hydrologic model and the quality of precipitation data to constrain uncertainties in simulated SWC to increase our confidence on the assessment of the effects of SWC changes on regional C balance.

Although the model was able to capture the temporal trends of annual streamflow at most areas, the existing disagreement between simulated and observed streamflow implies uncertainness in simulated SWC. Especially, the model tended to underestimate high streamflow values. It means that SWC might be overestimated in years with high streamflow. Consequently, C sequestration might be overestimated in poorly drained areas and underestimated in well-drained areas. In addition, errors in other input datasets might result in uncertainties in simulated C sequestration. For example, the land cover map was produced using remote sensing data and forest stand age map was a combination of large fire scar and remote sensing data. In a previous study conducted by Chen et al. (2003) showed that an error of 20% in land cover map might induces uncertainties of 2% and 0.5% in NBP and NPP during 1990–1998, respectively. However, the errors of 5 years in forest age caused uncertainties of 12–22% and 5–9% in simulated NBP and NPP, respectively. Therefore, a reliable forest stand age map is critical for increasing our confidence on the estimation of current regional C budget. In this study, forests were assumed to regenerate in the next year following disturbances. This simplification might artificially reduce C sources after disturbances.

The simulations show that SWC increased overall from 1901 to 2000 in most areas of Canada's forests and wetlands. In the Southern Taiga Plains, the Northwestern Boreal Plains, the Eastern Hudson Plains, the Eastern Middle Boreal shield ecozones and parts of the Southern Boreal Shield ecozone, SWC increased at the 1% significance level, owning to the fact that precipitation increased more than ET. In other areas, SWC increased less or even partially decreased at the 1% significance level. These areas include parts of the Taiga Shield, Taiga Cordillera, Taiga Plains and Boreal Cordillera ecozones. Starting from the 1970s, Canada's forests and wetlands experienced soil drying. SWC decreased extensively during 1971 to 2000.

The changes in SWC caused NPP to decrease by 4.9% (40.8 Tg C yr^{-1}) when averaged over the period from 1901 to 2000. The overall reduction of NPP is caused by the decrease in N mineralization under the condition of high SWC. N mineralization in Canada's forests and wetlands is low due to low temperature and anaerobic conditions of soils. During the middle 1940s to the middle 1970s, the reduction of N mineralization owing to increased SWC caused a large decrease in NPP. As the soil became progressively drier from the middle 1970s, N mineralization increased, leading to an increase in NPP in poorly drained areas. The SWC-induced reduction in NPP was exceeded by the SWC-induced decrease in heterotrophic respiration. Increases in SWC increased NBP of Canada's forests and wetlands by 4.1 Tg C yr^{-1} when averaged over the period from 1901 to 2000, which is relatively small compared with an increase of 50.2 Tg C yr^{-1} in NBP caused by the integrated effect of climate change, CO_2 fertilization and N deposition.

The increase in SWC resulted in increases in NBP in all ecozones because the increase in SWC caused more reduction in heterotrophic respiration than in NPP, implying that if the decreasing trend of SWC starting from the early 1970s continues, the current C sink of Canada's forests and wetlands will shrink. The C stock in Canada's forests and wetlands is huge. Future decreases in SWC caused by global warming might result in considerable increase in C released into the atmosphere from soils, intensifying climate change.

SWC affects two major components of the C cycle. Small errors in the simulated SWC and water table depth could induce a considerable error in simulated C budget at regional and/or global scales. However, hydrological processes are simplified in terrestrial C models due to data limitation and our limited knowledge on soil water movement. More efforts to simulate the water cycle and its effects on C cycling are needed to project the response of the terrestrial C cycle to future climate change.

7. Conclusions

The coupling between water and carbon cycles in Canada's forests and wetlands was studied through a series of numerical simulations with the InTEC model. Following conclusions can be drawn from this study:

(1) SWC in Canada's forests and wetlands varied spatially and temporally during 1901–2000. SWC increased at 1% significance level in the Southern Taiga Plains, Northwestern Boreal Plains, Eastern Hudson Plains, Eastern Middle Boreal Shield ecozones and parts of the Southern Boreal Shield ecozone and it significantly decreased in parts of the Taiga Shield, Taiga Cordillera, Taiga Plains and Boreal cordillera ecozones. The SWC decrease was widespread during 1971–2000, and significant at the 1% level in the Northern Taiga Plains, Southern Boreal Plains ecozones, the middles of the Hudson Plains and Southern Boreal Shield ecozones and parts of the Eastern Taiga Shield ecozone.

(2) During the simulation period of 100 years, SWC change alone caused a reduction in annual NPP of 40.8 Tg C yr^{-1}, while the integrated effect of climate change, CO_2 fertilization and N deposition enhanced NPP by 83.4 Tg C yr^{-1}, with 16.7 and 29.6 Tg C yr^{-1} enhancement from CO_2 fertilization and N deposition, respectively. The change of SWC increased net C uptake by of 4.1 Tg C yr^{-1}, relatively small compared with an enhancement of 50.2 Tg C yr^{-1} by the integrated effect of climate change, CO_2 fertilization and N deposition. The increase in SWC resulted in an increase in the net C uptake in all ecozones. The drop of SWC in 1998 caused heterotrophic respiration to increase by 100 Tg C yr^{-1}.

(3) In addition to enhancing heterotrophic respiration by increasing temperature, climate change might regulate C uptake by terrestrial ecosystems through its influence on SWC. Our simulations show that an increase in SWC would enhance net C sequestration in all ecozones in Canada due to the abundance of poorly drained areas in Canada's forests and wetlands, in which wetting of soils inhibited microbial activities, leading to reduction in heterotrophic respiration. Soil C storage in these areas is very large. Future possible decrease of SWC caused by increasing temperature and decreasing precipitation might increase C release to the atmosphere and have positive feedbacks to global warming.

Acknowledgements

We are indebted to Dr. Josef Cihlar of the Canada Centre for Remote Sensing for the use of the Canada-wide land cover map and to Agriculture and Food Canada for the Soil Landscape of Canada. We thank the Fluxnet-Canada Research Network and their sponsors for financial support. This study was also supported by the National High Technology Research and Development Program of China (2009AA122005) and Doctoral Fund of Ministry of Education of China (20090091110034).

Appendix A: The calculations of GPP and NPP

A.1. Calculation of NPP

Actual NPP of a forest is calculated as follows:

$$NPP(i) = NPP_u(i) Fnpp(i) \tag{A1}$$

where $NPP_u(i)$ is the NPP value determined by non-disturbance factors (climate, CO_2 concentration and N availability), $Fnpp(i)$ is the normalized forest productivity changing with stand age and ranges from 0 to 1.0 (Chen et al., 2000c).

The value of $NPP_u(i)$ is calculated through iteration

$$\begin{aligned}\frac{NPP_u(i) - NPP_u(i-1)}{NPP_u(i) + NPP_u(i-1)} &= \frac{GPP(i) - GPP(i-1) - R_a(i) + R_a(i-1)}{GPP(i) + GPP(i-1) - R_a(i) - R_a(i-1)} \\ &= \frac{(X(i)-1) - \beta(i-1)(Y(i)-1)}{(X(i)+1) - \beta(i-1)(Y(i)+1)} = B(i).\end{aligned} \tag{A2}$$

Therefore,

$$NPP_u(i) = NPP_u(i-1)\frac{1 - B(i)}{1 + B(i)}, \tag{A3}$$

where $X(i)$ is the interannual variability of GPP in year i (unitless), which is calculated using eqs (A8) and (A9), $\beta(i-1)$ is the ratio of maintenance respiration to GPP in year $(i-1)$ (unitless), and $Y(i)$ is the interannual variability of maintenance respiration in year i (unitless).

A.2. Calculation of GPP

The canopy-level instantaneous photosynthesis rate is calculated as follows:

$$P_{can} = P_{can1} f_p + P_{can2}(1 - f_p), \tag{A4}$$

where P_{can1} and P_{can2} are canopy gross photosynthesis rates limited by electron transport and rubisco activity, respectively, and f_p is the fraction of canopy photosynthesis limited by P_{can1}.

Through upscaling Farquhar's biochemical model from leaf to canopy, P_{can1} and P_{can2} are calculated as:

$$\begin{cases} P_{can1} = (J_{sun} LAI_{sun} + J_{shad} LAI_{shad}) \dfrac{C_i - \Gamma}{4.5C_i + 10.5\Gamma}, \\ P_{can2} = V_m \dfrac{C_i - \Gamma}{C_i + k_{co}} LAI, \end{cases} \quad \text{(A5)}$$

where LAI, LAI_{sun} and LAI_{shad} are the total, sunlit and shaded leaf area index ($m^2\ m^{-2}$), respectively. J is the electron transport rate (μmol $CO_2\ m^{-2}\ s^{-1}$), V_m is the maximum carboxylation rate (μmol $CO_2\ m^{-2}\ s^{-1}$), C_i is the intercellular CO_2 concentration and is determined using the analytical method developed by Baldocchi (1994), and Γ is the leaf CO_2 compensation point, and k_{co} is a coefficient associated with enzyme kinetics (Bonan, 1995).

The annual gross photosynthesis rate of a forest in year i is then obtained through integrating P_{can} over the growing season:

$$GPP(i) = \int_t P_{can}(t)\,\mathrm{d}t. \quad \text{(A6)}$$

To reduce the requirement for input data and to constrain the uncertainty in the calculation of historical photosynthesis, $GPP(i)$ is calculated according to the relationship between the interannual variability and the external forcing factors (Chen et al., 2000c):

$$\frac{\mathrm{d}GPP(i)}{\mathrm{d}i} = \int_t \frac{\mathrm{d}P_{can}(t)}{\mathrm{d}i}\,\mathrm{d}t + P_{can}(t)\frac{\partial l_g}{\partial i}, \quad \text{(A7)}$$

where the first term at the right-hand side of the equation represents the effect on the interannual variability of GPP caused by changes in $P_{can}(t)$ and second term represents the effect caused by the change of growing season length (l_g).

From eq. (A7), annual $GPP(i)$ is calculated using a temporal scaling algorithm developed by Chen et al. (2000c), that is

$$GPP(i) = GPP(i-1)\frac{2+\chi(i)}{2-\chi(i)} = GPP(i-1)X(i), \quad \text{(A8)}$$

where $\chi(i)$ represents the integrated effect of climate, atmospheric CO_2 concentration, N and soil water content on annual photosynthesis and is given by

$$\begin{aligned} \chi(i) = \{ & f_p(i)[\xi_{L_{1,1}}\overline{L_{1,1}}(i)\Delta C_a + \xi_{L_{2,1}}\overline{L_{2,1}}(i)\Delta\alpha \\ & + \xi_{L_{3,1}}\overline{L_{3,1}}(i)\Delta\Gamma + \xi_{L_{5,1}}\overline{L_{5,1}}(i)\Delta J_{mt} \\ & + \xi_{L_{N1}}\overline{L_{N1}}(i)\Delta N_l(i) + \xi_{L_{l1,1}}\overline{L_{L1,1}}(i)\Delta L_{sun}(i) \\ & + \xi_{L_{l1,2}}\overline{L_{L1,2}}(i)\Delta L_{shad}(i)] + (1 - f_p(i))[\xi_{L_{1,2}}\overline{L_{1,2}}(i)\Delta C_a \\ & + \xi_{L_{2,2}}\overline{L_{2,2}}(i)\Delta\alpha + \xi_{L_{3,2}}\overline{L_{3,2}}(i)\Delta\Gamma + \xi_{L_{4,2}}\overline{L_{4,2}}(i)\Delta k_{co} \\ & + \xi_{L_{5,2}}\overline{L_{5,2}}(i)\Delta V_{mt} + \xi_{L_{N2}}\overline{L_{N2}}(i)\Delta N_l(i)]\} + L_g\Delta l_g, \end{aligned} \quad \text{(A9)}$$

where Δx represents the interannual variability of variable x, ξ_{L_x} is a coefficient to correct the effect of diurnal and seasonal variations of L_x and P_{can} on dP and to correct the bias from the replacement of the temporal average of L_x by $\overline{L_x}$, which is calculated from the mean values of environmental variables. The formulations for calculating $\overline{L_x}$ terms in eq. (A9) are introduced in Ju et al. (2007).

A.3. Calculation of maintenance respiration

Annual maintenance respiration is calculated as follows:

$$R_a(i) = (C_l R_{l,15} + C_s R_{s,15} + C_{cr} R_{cr,15} + C_{fr} R_{fr,15}) Q_{10}^{\frac{T_a(i)-15}{10}}, \quad \text{(A10)}$$

where C_l, C_S, C_{cr} and C_{fr} are respiratory C in foliage, sapwood, coarse root and fine root biomass pools (g C m^{-2}), respectively; $R_{l,15}$ $R_{s,15}$ $R_{cr,15}$ and $R_{fr,15}$ are their respective annual respiration rates at an annual mean temperature of 15 °C (g C g^{-1} C yr^{-1}); $T_a(i)$ is annual mean temperature in year i (°C); and Q_{10} is the sensitivity of maintenance respiration to temperature, being a constant value of 2.3 for all biomass C pools. The change of Q_{10} with temperature and effects of root N content and SWC on root mantainance respiration were not included yet.

A.4. Calculation of heterotrophic respiration

Soil C and N dynamics are simulated using a modified approach of CENTURY (Parton et al., 1993; Ju and Chen, 2005). Soil C is split into nine pools: (1) surface structural litter, (2) soil structural litter, (3) woody litter, (4) surface metabolic litter, (5) soil metabolic litter, (6) surface microbial, (7) soil microbial, (8) slow and (9) passive. Heterotrophic respiration R_h is calculated as the sum of C released to the atmosphere from these nine C pools during the decomposition of soil C:

$$R_h(i) = \sum_{j=1}^{9} k_j(i)\varepsilon_j C_j(i), \quad \text{(A11)}$$

where $k_j(i)$ is the decomposition rate of soil C pool j in year i(yr^{-1}) and calculated as a function of the prescribed maximum decomposition coefficient (Parton et al., 1993), soil temperature, soil moisture, soil texture (for pool 7), lignin content (for pools 1, 2 and 3) and N availability (for pools 1, 2, 3, 4, 5, 8 and 9) (Ju et al., 2007); ε_j is the prescribed fraction of decomposed C respired to the atmosphere from pool j; and $C_j(i)$ is the size of soil C pool j in year i (g C m^{-2}).

A.5. Simulation of C dynamics

The balance of each C pool is calculated as the difference between inputs and outputs. Annual NPP is partitioned into four biomass C pools (foliage, stem, coarse root and fine root) at the end of a year:

$$\Delta C_j(i) = (f_j NPP(i) - \eta_j C_j(i))/(1 + \eta_j), \quad \text{(A12)}$$

where f_j and η_j are the prescribed allocation coefficient of NPP to biomass pool j and the turnover rate of biomass pool j (yr^{-1}), respectively. They depend on land cover type.

Soil C pools are updated as follows:

$$\Delta C_j(i) = \left(\sum_{l=1}^{n} k_{l,j}(i) C_l(i-1) - k_j(i) C_j(i-1) \right) / (1 + k_j(i)), \quad \text{(A13)}$$

where n is number of C pools transferring C to pool j, $k_{l,j}(i)$ is transfer rate of C from pool l to pool j in year i(yr^{-1}), $k_j(i)$ is the decomposition rate of pool j in year i(yr^{-1}) and $C_1(i-1)$ and $C_j(i-1)$ are pool sizes in year $(i-1)$, respectively.

The scalar representing the effect of SWC on soil C decomposition $M_s(i, m)$ (unitless) is

$$M_s(i, m) = 5.44\theta(i, m) - 5.03\theta^2(i, m) - 0.472, \quad \text{(A14)}$$

where $\theta(i, m)$ is SWC expressed as the fraction of porosity in month m of year i. The minimum of $M_s(i,m)$ is set as 0.1.

The scalar of soil temperature affecting soil C decomposition $M_t(i, m)$ (unitless) is (Lloyd and Taylor, 1994):

$$M_t(i, m) = e^{308.56\left(\frac{1}{35+46.02} - \frac{1}{T_s(i,m)+46.02}\right)}, \quad \text{(A15)}$$

where $T_s(i, m)$ is soil temperature in month m of year i (°C).

A.6. *Simulation of nitrogen cycle*

N transformations among various litter and soil C pools follow C flows. N available for vegetation uptake is the sum of fixation N_{fix}, deposition N_{dep} and net mineralization N_{min}:

$$N_{av}(i) = N_{fix}(i) + N_{dep}(i) + N_{min}(i), \quad \text{(A16)}$$

N fixation is a function of temperature, precipitation and microbial biomass:

$$N_{fix}(i) = c_1 2.0^{T_s(i)/10} APPT(i)/0.45 \times (C_{sm}(i) + C_m(i))/200, \quad \text{(A17)}$$

where c_1 is a coefficient determining the fixation rate (0.15 g N m^{-2} yr^{-1}), $T_s(i)$ is annual mean soil temperature (°C), $APPT(i)$ is annual precipitation (m), and $C_{sm}(i)$ and $C_m(i)$ are sizes of surface and soil microbial C pools (g C m^{-2}), respectively.

N deposition is interpolated for each year according to rates of N deposition in a reference year i_{ref} (including dry and wet deposition) and the increase rate of greenhouse gas emission:

$$N_{dep}(i) = N_{dep}(0) + \frac{[N_{dep}(i_{ref}) - N_{dep}(i_0)][G(i) - G(i_0)]}{[G(i_{ref}) - G(i_0)]}, \quad \text{(A18)}$$

where N_{dep} is the N deposition rate (g N m^{-2} yr^{-1}), G is the greenhouse gas emission rate (Tg yr^{-1}) and i_0, i_{ref} and i represent the initial year, the reference year and a simulation year, respectively.

Net N mineralization is calculated according to C flows and C/N ratios of soil C pools (Ju et al., 2007).

The amount of N available $N_{av}(i)$ for forest uptake is the sum of fixation, deposition and net mineralization:

N uptake by forest $N_{up}(i)$ (g N m^{-2}) is determined by N availability and fine root mass $C_{fr}(i)$:

$$N_{up}(i) = \frac{N_{av}(i)}{1 + bN_{av}(i)/C_{fr}(i)}, \quad \text{(A19)}$$

where b is a coefficient determining the maximum uptake capacity of a forest (Chen et al., 2000b).

SWC affects the simulated GPP in two ways. If soils are too wet (SWC above field capacity), the decrease of SWC will enhance N mineralization, resulting in increase in GPP. When SWC is below field capacity, soil drying will cause reductions in both N mineralization and stomatal conductance. Consequently, GPP will be reduced.

Appendix B: The hydrological model

B.1. *Calculation of canopy transpiration and soil evaporation*

Evapotranspiration is calculated as the sum of canopy transpiration, evaporation from intercepted water and from soil surface and sublimation from intercepted snow and snowpack on the ground.

Canopy transpiration is separately calculated for sunlit and shaded leaves:

$$T_{rp,c} = T_{rp,sun} LAI_{sun} + T_{rp,shaded}(LAI - LAI_{sun}), \quad \text{(B1)}$$

where $T_{rp,c}$ is the total transpiration from the canopy (m d^{-1}); $T_{rp,sun}$ and $T_{rp,shaded}$ are daily transpiration per unit sunlit and shaded leaves (m d^{-1}), respectively, and calculated using the Penman–Monteith equation; LAI is leaf area index ($m^2 m^{-2}$) and LAI_{sun} is the sunlit leaf area index (m^2 m^{-2}) (Liu et al., 2003). In the calculation of transpiration, the stomatal resistance of individual leaves is calculated using the Ball–Berry model (Ball et al., 1987) which is solved analytically following Baldocchi (1994).

Evaporation from the intercepted water and the soil surface is also calculated using the Penman–Monteith equation, but different surface resistance values are used. For intercepted water, r_s is set to zero. Soil evaporation is calculated using an r_s value of 150 s m^{-1}.

Canopy transpiration and soil evaporation are down scaled by a soil water stress factor, which is given by a simple heuristic function (Foley et al., 1996):

$$f(w) = (1 - e^{-c\frac{\theta - \theta_w}{1 - \theta_{ws}}})/(1 - e^{-c}), \quad \text{(B2)}$$

where c is a parameter determining the sensitivity of transpiration and soil evaporation to soil water stress and a constant of 2.5 is used in this study, θ is the soil water content expressed as the fraction of the soil porosity θ_s, θ_w is the wilting point expressed as the fraction of the soil porosity.

B.2. Simulation of soil water content

Soil water content is updated as follows:

$$\frac{\partial\theta_1}{\partial t}\theta_{s1} = \frac{1}{d_1}(W_I - T_{r1} - E_s - Q_{1,2} - RF), \tag{B3a}$$

$$\frac{\partial\theta_2}{\partial t}\theta_{s2} = \frac{1}{d_2}(Q_{1,2} - T_{r2} - Q_{2,3}), \tag{B3b}$$

$$\frac{\partial\theta_3}{\partial t}\theta_{s3} = \frac{1}{d_3}(Q_{2,3} - T_{r3} - Q_3 - D_r), \tag{B3c}$$

where θ_i is the simulated SWC expressed as the fraction of the soil porosity in soil layer i, θ_{si} is the soil porosity of layer i (m^3 m^{-3}), d_i is the thickness of soil layer i (m), W_I is total water input to the first soil layer, including through fall of rain and snow melt (m d^{-1}), T_{ri} is transpiration uptake from layer i (m d^{-1}), E_s is evaporation from the first soil layer (m d^{-1}), RF is surface runoff (m d^{-1}), $Q_{i,i+1}$ is vertical percolation of soil water from layer i to layer $(I + 1)$ (m d^{-1}); Q_3 is horizontal saturated subsurface flow (m d^{-1}), which is designated to link individual pixel hydrologically with the neighbouring pixels and D_r is bottom drainage (m d^{-1}). The water leaving a watershed is calculated as the sum of surface runoff RF and bottom drainage D_r.

The simulation of SWC is conducted two times in a time step. First, only vertical water fluxes are computed to solve for the SWC of each soil layer. Then, lateral saturated base flow Q_3 is calculated and SWC is adjusted according to the value of Q_3 (Ju and Chen, 2005).

B.3. Surface runoff and bottom drainage

Surface runoff RF_t is estimated as follows:

$$RF_t = W_I R_{r,t}, \tag{B4}$$

where $R_{r,t}$ is the runoff fraction of rain throughfall and snowmelt and is estimated as a function of the SWC in the first soil layer:

$$\begin{aligned} R_{r,t} &= (1 - B)\left(\frac{\theta_{1,t} - \theta_{w1}}{1 - \theta_{w1}}\right)^A + B\left(\frac{\theta_{1,t+1} - \theta_{w1}}{1 - \theta_{w1}}\right)^A \\ &= a_0 + a_1\theta_{1,t+1}, \end{aligned} \tag{B5}$$

where t is the time step, B is the weight given to implicit formulation ($B = 0$ for the purely explicit solution, $B = 0.5$ for the Crank–Nicolson solution, and $B = 1.0$ for the purely implicit solution), A is the sensitivity of runoff to SWC depending on soil drainage condition, $a_0 = (\frac{\theta_{1,t} - \theta_{w1}}{1 - \theta_{w1}})^A - \frac{AB}{1-\theta_{w1}}\left(\frac{\theta_{1,t} - \theta_{w1}}{1 - \theta_{w1}}\right)^{A-1}\theta_{1,t}$ and $a_1 = \frac{AB}{1-\theta_{w1}}(\frac{\theta_{1,t} - \theta_{w1}}{1 - \theta_{w1}})^{A-1}$.

Drainage from the bottom of the soil profile is

$$\begin{aligned} D_r &= (1 - B)K_3(\theta_{3,t})^m + BK_3(\theta_{3,t+1})^m \\ &= c_0 + c_1\theta_{3,t+1}, \end{aligned} \tag{B6}$$

where K_3 is the saturated hydraulic conductivity of soil layer 3 (m d^{-1}), and $m = 2b + 3$, where b is the exponent of the soil moisture release equation; further, $c_0 = K_3(\theta_{3,t})^m(1 - Bm)$ and $c_1 = BmK_3(\theta_{3,t})^{m-1}$.

B.4. Transpiration from different soil layers

Transpiration consumption is proportioned among soil layers according to a soil water stress factor and root abundance:

$$T_{ri} = T_{tp,c}r_i[(1 - B)f(w_{i,t}) + Bf(w_{i,t+1})], \tag{B7}$$

where r_i is the fraction of roots in layer i.

Inserting eq. (B2) into eq. (B7), transpired water from layer i is approximated as follows:

$$\begin{aligned} T_{ri} &= T_{tp,c}r_i\frac{1}{1 - e^{-c}}[(1 - e^{-c\frac{\theta_{i,t} - \theta_{wi}}{1-\theta_{wi}}}) \\ &\quad + \tfrac{cB}{1-\theta_{wi}}e^{-c\frac{\theta_{i,t} - \theta_{wi}}{1-\theta_{wi}}}(\theta_{i,t+1} - \theta_{i,t})] \\ &= b_{0,,i} + b_{1,i}\theta_{i,t+1}, \end{aligned} \tag{B8}$$

where

$$b_{0,i} = T_{tp,c}r_i\frac{1}{1 - e^{-c}}\left[\left(1 - e^{-c\frac{\theta_{i,t} - \theta_{wi}}{1-\theta_{wi}}}\right) - \frac{cB}{1 - \theta_{wi}}e^{-c\frac{\theta_{i,t} - \theta_{wi}}{1-\theta_{wi}}}\theta_{i,t}\right]$$

and

$$b_{1,i} = T_{tp,c}r_i\frac{cB}{(1 - e^{-c})(1 - \theta_{wi})}e^{-c\frac{\theta_{i,t} - \theta_{wi}}{1-\theta_{wi}}}.$$

Vertical water percolation is simulated by implicitly solving the Darcy's equation

$$\begin{aligned} Q_{i,i+1} &= (1 - B)K_{i,i+1}\left[(\vartheta_{i,i+1,t})^{m_{i,i+1}}\right. \\ &\quad \left. + \psi_{i.,i+1}b_{i,i+1}(\vartheta_{i,i+1,t})^{n_{i,i+1}}\frac{\theta_{i,t} - \theta_{i+1,t}}{D_{i,i+1})}\right] \\ &\quad + BK_{i,i+1}\left[(\vartheta_{i,i+1,t+1})^{m_{i,i+1}}\right. \\ &\quad \left. + \psi_{i.,i+1}b_{i,i+1}(\vartheta_{i,i+1,t+1})^{n_{i,i+1}}\frac{\theta_{i,t+1} - \theta_{i+1,t+1}}{D_{i,i+1})}\right], \end{aligned} \tag{B9}$$

where $K_{i,i+1}$, $\psi_{i,i+1}$ and $\vartheta_{i,i+1}$ are the saturated hydraulic conductivity, suction at air entry and SWC at the boundary of soil layers i and $i + 1$, respectively; $m_{i,i+1}$ and n_{i+1} are two parameters dependent on b; and $D_{i,i+1}$ is the vertical distance between the centres of layers i and $i+1$. Variables on the right side of eq. (B11) are computed as follows:

$$K_{i,i+1} = 0.5(K_i d_{i+1}/D_{i,i+1} + K_{i+1}d_i/D_{i,i+1}), \tag{B10a}$$

$$\psi_{i,i+1} = 0.5(\psi_i d_{i+1}/D_{i,i+1} + \psi_{i+1}d_i/D_{i,i+1}), \tag{B10b}$$

$$\vartheta_{i,i+1} = 0.5(\theta_i d_{i+1}/D_{i,i+1} + \theta_{i+1}d_i/D_{i,i+1}), \tag{B10c}$$

$$m_{i,i+1} = (b_i d_{i+1}/D_{i,i+1} + b_{i+1}d_i/D_{i,i+1}) + 3, \tag{B10d}$$

$$n_{i,i+1} = 0.5(b_i d_{i+1}/D_{i,i+1} + b_{i+1}d_i/D_{i,i+1}) + 2. \tag{B10e}$$

Using the first order Taylor series to approximate the second term on the right side of eq. (B9), this equation can be rewritten as follows:

$$Q_{i,i+1} = (1 - Bm_{i,i+1})K_{i,i+1}(\vartheta_{i,i+1,t})^{m_{i,i+1}} + \begin{bmatrix} (1-B) + Bn_{i,i+1}]K_{i,i+1}\psi_{i,i+1}b_{i+1}\frac{\theta_{i,t}-\theta_{i+1,t}}{D_{i,i+1}} \\ + BK_{i,i+1}\big[m_{i,i+1}(\vartheta_{i,i+1,t})^{m_{i,i+1}-1} \\ + n_{i,i+1}\psi_{i,i+1}b_{i,i+1}(\vartheta_{i,i+1,t})^{n_{i,i+1}-1} \\ \times \frac{\theta_{i,t}-\theta_{i+1,t}}{D_{i,i+1}}\big]\vartheta_{i,i+1,t+1} \\ + B\psi_{i,i+1}b_{i,i+1}(\vartheta_{i,i+1,t})^{n_{i,i+1}}\frac{\theta_{i,t+1}-\theta_{i+1,t+1}}{D_{i,i+1}} \end{bmatrix}. \quad \text{(B11)}$$

B.5. *Solving for soil water content in different soil layers*

Combing eqs (B3), (B7), (B8) and (B11), eq. (B3) can be expressed in the following manner for updating the SWC (Q_3 is excluded at this simulation step)

$$\begin{bmatrix} x_{11} & x_{12} & 0 \\ x_{21} & x_{22} & x_{23} \\ 0 & x_{32} & x_{33} \end{bmatrix} \begin{bmatrix} \theta_{1,t+1} \\ \theta_{2,t+1} \\ \theta_{3,t+1} \end{bmatrix} = \begin{bmatrix} y_1 \\ y_2 \\ y_3 \end{bmatrix}. \quad \text{(B12)}$$

In the simulations of SWC, the influences of temperature on soil water movement is corrected following Sellers et al. (1996), assuming saturated hydraulic conductivity linearly decreases with temperature decrease when soil is frozen.

Appendix C

Temperatures of the soil and snow pack are simulated using the implicit solution of Fick's law of heat diffusion

$$\frac{C_i h_i[Ts_{i,t+1} - Ts_{i,t}]}{86400\Delta t} = 2\Bigg\{(1-B)\Bigg[\frac{Ts_{i-1,t} - Ts_{i,t}}{d_{i-1}/\lambda_{i-1} + d_i/\lambda_i} - \frac{Ts_{i,t} - Ts_{i+1,t}}{d_i/\lambda_i + d_{i+1}/\lambda_{i+1}}\Bigg] + B\Bigg[\frac{Ts_{i-1,t+1} - Ts_{i,t+1}}{d_{i-1}/\lambda_{i-1} + d_i/\lambda_i} - \frac{Ts_{i,t+1} - Ts_{i+1,t+1}}{d_i/\lambda_i + d_{i+1}/\lambda_{i+1}}\Bigg]\Bigg\}. \quad \text{(C1)}$$

where C is the apparent volumetric heat capacity (J m^{-3} K), d is the depth of layer (m), Ts represents soil temperature (°C), Δt is the number of days per month and λ is the thermal conductivity (W m^{-1} K^{-1}); and subscripts i and t denote the soil layer and the time step, respectively.

For soil temperature simulation, the number of layers changes seasonally. If the depth of snowpack is above 5 cm, a snow layer is explicitly included. Otherwise, the snowpack is lumped with the first soil layer. The thermal properties of the first layer are adjusted according to the amount of snow. For the first soil layer or snow layer, $Ts_{i-1,t+1}$ is set to the ground surface temperature, which is converted from monthly mean air temperature using an empirical equation based on the leaf are index (Yin and Arp, 1993). We assume that heat flux is zero at the bottom of the soil profile.

Equation (C1) can be rewritten in the format similar to eq. (B12). Temperatures of three soil layers and snow pack can be solved simultaneously.

References

Amiro, B. D. and Chen J. M. 2003. Forest-fire-scar aging using spot-vegetation for Canadian ecoregions. *Can. J. Forest Res.* **33**, 1116–1125.

Arain, M. A., Black, T. A., Barr, A. G., Jarvis, P. G., Massheder, J. M. and co-authors. 2002. Effects of seasonal and interannual climate variability on net ecosystem productivity of boreal deciduous and conifer forests. *Can. J. Forest Res.* **32**, 878–891.

Arora, V. K. 2003. Simulating energy and carbon fluxes over winter wheat using coupled land surface and terrestrial ecosystem models. *Agric. Forest Meteorol.* **118**, 21–47.

Baldocchi, D. D. 1994. An analytical solution for coupled leaf photosynthesis and stomatal conductance models. *Tree Physiol.* **14**, 1069–1079.

Ball, J. T., Woodrow, I. E. and Berry, J. A. 1987. A model predicting stomatal conductance and its contribution to the control of photosynthesis under different environmental conditions. In: *Progress in Photosynthesis Research* (ed. J. Biggins). Martinus Nijhoff Publishers, Dordrecht, the Netherlands, 221–224.

Barr, A. G., Black, T. A., Hogg, E. H., Kljun, N., Morgenstern, K. and co-authors. 2004. Inter-annual variability in the leaf area index of a boreal aspen-hazelnut forest in relation to net ecosystem production. *Agric. Forest Meteorol.* **126**, 237–255.

Black, T. A., Chen, W. J., Barr, A. G., Arain, M. A., Chen, Z. and co-authors. 2000. Increased carbon sequestration by a boreal deciduous forest in years with a warm spring. *Geophys. Res. Lett.* **27**, 1271–1274.

Black, T. A., Denhartog, G., Neumann, H. H., Blanken, P. D., Yang, P. C. and co-authors. 1996. Annual cycles of water vapour and carbon dioxide fluxes in and above a boreal aspen forest. *Global Change Biol.* **2**, 219–229.

Bonan, G. B. 1995. Land atmosphere interactions for climate system models – coupling biophysical, biogeochemical, and ecosystem dynamical processes. *Remote Sens. Environ.* **51**, 57–73.

Borken, W., Davidson, E. A., Savage, K., Gaudinski, J. and Trumbore S. E. 2003. Drying and wetting effects on carbon dioxide release from organic horizons. *Soil Sci. Soc. Am. J.* **67**, 1888–1896.

Brown, S. L. and Schroeder P. E. 1999. Spatial patterns of aboveground production and mortality of woody biomass for eastern us forests. *Ecol. Appl.* **9**, 968–980.

Campbell, G. S. and Norman J. M. 1998. *An Introduction to Environmental Biophysics*, Springer-Verlag, New York, 129–144.

Caspersen, J. P., Pacala, S. W. J., Jenkins, C., Hurtt, G. C., Moorcroft, P. R. and co-authors. 2000. Contributions of land-use history to carbon accumulation in us forests. *Science* **290**, 1148–1151.

Chen, J. M., Liu, J., Cihlar, J. and Goulden, M. L. 1999. Daily canopy photosynthesis model through temporal and spatial scaling for remote sensing applications. *Ecol. Modell.* **124**, 99–119.

Chen, J., Chen, W. J., Liu, J., Cihlar, J. and Gray S. 2000a. Annual carbon balance of Canada's forests during 1895–1996. *Global Biogeochem. Cycles* **14**, 839–849.

Chen, W.J., Chen, J. M. and Cihlar, J. 2000b. An integrated terrestrial ecosystem carbon-budget model based on changes in disturbance, climate, and atmospheric chemistry. *Ecol. Modell.* **135**, 55–79.

Chen, W. J., Chen, J. M., Liu, J. and Cihlar, J. 2000c. Approaches for reducing uncertainties in regional forest carbon balance. *Global Biogeochem. Cycles* **14**, 827–838.

Chen, J. M., Ju, W. M., Cihlar, J., Price, D., Liu, J. and co-authors. 2003. Spatial distribution of carbon sources and sinks in Canada's forests. *Tellus* **B55**, 622–641.

Ciais, P., Reichstein, M., Viovy, N., Granier, A., Ogee, J. and co-authors. 2005. Europe-wide reduction in primary productivity caused by the heat and drought in 2003. *Nature* **437**, 529–533.

Cihlar, J., Xiao, Q., Chen, J. M., Beaubien, J., Fung K. and co-authors. 1998. Classification by Progressive Generalization: a new automated methodology for remote sensing multichannel data. *Int. J. Remote Sens.* **19**, 2685–2704.

Dai, A. and I. Y. Fung 1993. Can climate variability contribute to the "missing" CO_2 sink? *Global Biogeochem. Cycles* **7**(3), 599–609.

Davidson, E. A., Belk, E. and Boone, R. D. 1998. Soil water content and temperature as independent or confounded factors controlling soil respiration in a temperate mixed hardwood forest. *Global Change Biol.* **4**, 217–227.

Davis, R. E., Michael, B. L. and Knappenberger P. C. 1999. A climatology of snowfall-temperature relationships in Canada. *J. Geophys. Res.* **D104**, 11985–11994.

Dunn, A. L., Barford, C. C., Wofsy, S. C., Golden, M. L. and Daube B. C. 2007. A long-term record of carbon exchange in a boreal black spruce forest: means, responses to interannual variability, and decadal trends. *Global Change Biol.* **13**(3), 577–590.

Friend, A. D., Stevens, A. K., Knox, R. G. and Cannell, M. G. R. 1997. A process-based, terrestrial biosphere model of ecosystem dynamics (Hybrid V3.0). *Ecol. Modell.* **95**, 249–287.

Frolking, S., Roulet, N. T., Moore, T. R., Richard, P. J. H., Lavoie, M. and co-authors. 2001. Modeling northern peatland decomposition and peat accumulation. *Ecosystems* **4**, 479–498.

Foley, J. A., Prentice, I. C., Ramankutty, N., Levis, S., Pollard, D. and co-authors. 1996. An integrated biosphere model of land surface processes, terrestrial carbon balance, and vegetation dynamics. *Global Biogeochem. Cycles* **10**, 603–628.

Goulden, M.L., Munger, J. W., Fan, S. M., Daube, B. C. and Wofsy, S. C. 1996. Exchange of carbon dioxide by a deciduous forest: response to interannual climate variability. *Science* **271**(5255), 1576–1578.

Gorham E. 1995. The biogeochemistry of northern peatlands and its possible response to global warming. In: *Biotic feedbacks in the Global Climatic System: Will the Warming Feed the Warming?* (eds G. M. Woodwell and F. T. Mackenzie). Oxford University Press, New York, 169–187.

Griffis, T. J., Black, T. A., Morgenstern, K., Barr, A. G., Nesic, Z. and co-authors. 2003. Ecophysiological controls on the carbon balances of three southern boreal forests. *Agric. Forest Meteorol.* **117**, 53–71.

Holland, E. A., Braswell, B. H., Lamarque, J. F., Townsend, A., Sulzman, J. and co-authors. 1997. Variations in the predicted spatial distribution of atmospheric nitrogen deposition and their impact on carbon uptake by terrestrial ecosystems. *J. Geophys. Res.* **D102**, 15849–15866.

Humphreys, E. R., Black, T. A., Ethier, G. J., Drewitt, G. B., Spittlehouse, D. L. and co-authors. 2003. Annual and seasonal variability of sensible and latent heat fluxes above a coastal Douglas-fir forest, British Columbia, Canada. *Agric. Forest Meteorol.* **115**, 109–125.

Humphreys, E. R., Lafleur, P. M., Admiral, S. W. and Roulet N. T. 2004. Contrasting the interannual variability in net ecosystem exchange of carbon dioxide in a northern peatland with the variability observed in northern forests. In: *Proceedings of the 26th Conference on Agricultural and Forest Meteorology*, August 23–27, Vancouver, BC, Canada.

Infante, J. M., Damesin, C., Rambal, S. and Fernandez-Ales, R. 1999. Modelling leaf gas exchange in holm-oak trees in southern Spain. *Agric. Forest Meteorol.* **95**, 203–223.

Jarvis, P. G., Massheder, J. M., Hale, S. E., Moncrieff, J. B., Rayment, M. and co-authors. 1997. Seasonal variation of carbon dioxide, water vapor, and energy exchanges of a boreal black spruce forest. *J. Geophys. Res.* **D102**, 28953–28966.

Ju, W. M. and Chen J. M. 2005. Distribution of soil carbon stocks in Canada's forests and wetlands simulated based on drainage class, topography and remotely sensed vegetation parameters. *Hydrol. Proc.* **19**, 77–94.

Ju, W. M., Chen, J. M., Black, T. A., Barr, A. G., McCaughey, J. H. and co-authors. 2006. Hydrological effects on C cycles of Canada's forests and wetlands. *Tellus* **58B**, 16–30.

Ju, W. M., Chen, J. W., Harvey, D. and Wang, S. Q. 2007. Future carbon balance of China's forests under climate change and increasing CO_2. *J. Environ. Manage.* **85**, 538–562.

Ju, W. M. and Chen, J. M. 2008. Simulating the effects of past changes in climate, atmospheric composition, and fire disturbance on soil carbon in Canada's forests and wetlands. *Global Biogeochem. Cycles* **22**, doi:10.1029/2007GB002935.

Kendall, M. K. 1975. *Rank Correlation Methods*. Charles Griffin, London.

Kljun N., Black, T. A., Griffis, T. J., Barr, A. G., Gaumont-Guay, D. and co-authors. 2006. Response of net ecosystem productivity of three boreal forest stands to drought. *Ecosystems* **9**(7), 1128–1144.

Kucharik, C. J., Foley, J. A., Delire, C., Fisher, V. A., Coe, M. T. and co-authors. 2000. Testing the performance of a dynamic global ecosystem model: water balance, carbon balance, and vegetation structure. *Global Biogeochem. Cycles* **14**, 795–825.

Kurz, W. A., Apps, M. J., Webb, T. M. and McNamee, P. J. 1992. The C budget of the Canadian forest sector: Phase I. Forestry Canada. Canadian Forest Service, Information Report. NOR-X-326.

Kurz W. A. and Apps M. J. 1999. A 70-year retrospective analysis of carbon fluxes in the Canadian forest sector. *Ecol. Appl.* **9**, 526–547.

Lafleur, P. M., Roulet, N. T., Bubier, J. L., Frolking, S. and Moore, T. R. 2003. Interannual variability in the peatland-atmosphere carbon dioxide exchange at an ombrotrophic bog. *Global Biogeochem. Cycles* **17**, doi:10.1029/2002GB001983.

Lal, R. 2005. Forest soils and carbon sequestration. *Forest Ecol. Manage.* **220**, 242–258.

Lawlor, D. W. 1995. The effects of water deficit on photosynthesis. In: *Environmental and Pant Metabolism-Flexibility and Acclimation* (ed N. Smirnoff). Bioscience Scientific Publishers, Oxford, 129–160.

Letts, M. G., Roulet, N. T., Comer, N. T., Skarupa, M. R. and Verseghy D. L. 2000. Parameterization of peatland hydraulic properties for the Canadian land surface scheme. *Atmos.-Ocean* **38**, 141–160.

Liu, J., Chen, J. M., Cihlar, J. and Chen, W. J. 2002. Net primary productivity mapped for Canada at 1-km resolution. *Global Ecol. Biogeogr.* **11**, 115–129.

Liu, J., Chen, J. M. and Cihlar, J. 2003. Mapping evapotranspiration based on remote sensing: an application to Canada's landmass. *Water Resour. Res.* **39**, 1189–1200.

Lloyd, J. and Talor J. A. 1994. On the temperature-dependence of soil respiration. *Funct. Ecol.* **8**, 315–323.

Mann, H. B. 1945. Non-parametric tests against trend. *Econometric* **13**, 245–259.

New, M., Hulme, M. and Jones, P. 1999. Representing twentieth-century space-time climate variability. Part I: development of a 1961–90 mean monthly terrestrial climatology. *J. Clim.* **12**, 829–856.

New, M., Hulme, M. and Jones, P. 2000. Representing twentieth-century space-time climate variability. Part II: development of 1901–96 monthly grids of terrestrial surface climate. *J. Clim.* **13**, 2217–2238.

Parton, W. J., Scurlock, J. M. O., Ojima, D. S., Gilmanov, T.G., Scholes, R. J. and co-authors. 1993. Observations and modelling of biomass and soil organic matter dynamics for grassland biome worldwide. *Global Biogeochem. Cycles* **7**, 785–809.

Prentice I. C., Farquhar, G. D., Fasham, M. J. R., Golden, M. L., Heiman, M. and co-authors. 2001. The carbon cycle and atmosphere carbon dioxide. In: Climate Change 2001: the Scientific Basis. Contribution of Working Group I to the Third Assessment Report of the Intergovernmental Panel on Climate Change, Cambridge University Press, Cambridge, UK.

Rambal, S., Ourcival, J. M., Joffre, R., Mouillot, F., Nouvellon, Y. and co-authors. 2003. Drought controls over conductance and assimilation of a Mediterranean evergreen ecosystem: scaling from leaf to canopy. *Global Change Biol.* **9**, 1813–1824.

Rapalee, G., Trumbore, S. E., Davidson, E. A., Harden, J. W. and Veldhuis, H. 1998. Soil carbon stocks and their rates of accumulation and loss in a boreal forest landscape. *Global Biogeochem. Cycles* **12**, 687–701.

Reichstein, M., Tenhunen, J. D., Roupsard, O., Ourcival, J. M., Rambal, S. and co-authors. 2002. Severe drought effects on ecosystem CO_2 and H2O fluxes at three Mediterranean evergreen sites: revision of current hypotheses?. *Global Change Biol.* **8**, 999–1017.

Ro, C., Vet, R., Ord, D. and Holloway, A. 1995. National Atmospheric Chemistry Database 1993. Annual report, acid precipitation in eastern Northern America, Atmospheric Environment Service, Environment Canada.

Saxton, K. E., Rawls, W. J., Romberger, J. S. and Papendick, R. I., 1986. Estimating generalized soil water characteristics from texture. *Soil Sci. Soc. Am. J.* **50**, 1031–1036.

Schimel, D., Melillo, J., Tian, H. Q., Mcguire, A. D., Kicklighter, D. and co-authors. 2000. Contribution of increasing CO_2 and climate to carbon storage by ecosystems in the United States. *Science* **287**, 2004–2006.

Schut, P., Shields, J., Tarnocai, C., Coote, D. and Marshall, I. 1994. Soil landscapes of Canada-an environmental reporting tool. In: *Canadian Conference on GIS Proceedings*, 6–10 June, 1994, pp. 953–965. Ottawa.

Sellers, P. J., Randall, D. A., Collatz, G. J., Berry, J. A., Field, C. B. and co-authors. 1996. A revised land surface parameteiztion (SiB2) for atmospheric GCMs. Part I: model formulation. *J. Clim.* 9, 676–795.

Siltanen, R. M., Apps, M. J., Zoltai, S. C., Mair, R. M. and Strong, W. L., 1997. *A Soil Profile and Organic C Data Base for Canadian Forest and Tundra Mineral Soils*. Canadian Forest Service, Ottawa, ON.

Tarnocai, C., Canadell, J. G., Schuur, E. A. G., Kuhry, P. M. and Zimov, S. 2009. Soil organic carbon pools in the northern circumpolar permafrost region. *Global Biogeochem. Cycles* **23**, GB2023, doi:10.1029/2008GB003327.

Thornton, P. E. and Running, S. W. 1999. An improved algorithm for estimating incident daily solar radiation from measurements of temperature, humidity, and precipitation. *Agric. Forest Meteorol.* **93**, 211–228.

Tolonen, K., Vasamder, H., Damman, A. W. H. and Clymo, R.S. 1992. Preliminary estimate of long term C accumulation and loss in 25 boreal peatlands. *Suo* **43**, 277–280.

Trumbore, S. E. and Harden, J. W. 1997. Accumulation and turnover of carbon in organic and mineral soils of the BOREAS northern study area. *J. Geophys. Res.* **102**(D24), 28817–28830, doi:10.1029/97JD02231.

Wigmosta, M. S., Vail, L. W. and Lettenmaier D. P. 1994. A distributed hydrology-vegetation model for complex terrain. *Water Resour. Res.* **30**, 1665–1679.

Zhang, X. B., Vincent, L. A., Hogg, W. D. and Niitsoo A. 2000. Temperature and precipitation trends in Canada during the 20th Century. *Atmos.-Ocean* **38**, 395–429.

Zhang, X. B., Harvey, K. D., Hogg, W. D. and Yuzyk, T.R. 2001. Trends in Canadian streamflow. *Water Resour. Res.* **37**, 987–998.

Zoltai, S. C., Tarnocai C., Mills, G. F. and Veldhuis H. 1988a. Wetlands of subarctic Canada. In: *Wetlands of Canada*. Ecological Classification Series, NO. 24. Sustainable Development Branch, Environmental Canada and Polyscience Publications, Montreal, Quebec.

Zoltai, S. C., Taylor, S., Jeglum, J. K., Mills, G. F. and Johnson, J. D. 1988b. Wetlands of boreal Canada. In: *Wetlands of Canada*. Ecological Classification Series, NO. 24. Sustainable Development Branch, Environmental Canada and Polyscience Publications, Montreal, Quebec.

Yin, X. W. and Arp, P. A. 1993. Predicting forest soil temperatures from monthly air-temperature and precipitation records. *Can. J. Forest Res.* **23**, 2521–2536.